University of Alberta

The Queen Maud Block, Nunavut - Genesis of a large felsic igneous province in the earliest Paleoproterozoic and implications for Laurentian geotectonic models

by

Michael E.J. Schultz 

A thesis submitted to the Faculty of Graduate Studies and Research in partial fulfillment of the requirements for the degree of Master of Science

Department of Earth and Atmospheric Sciences

Edmonton, Alberta

Fall 2007

Your file Votre référence
ISBN: 978-0-494-33343-3
Our file Notre référence
ISBN: 978-0-494-33343-3

University of Alberta

Library Release Form

Name of Author: Michael E.J. Schultz

Title of Thesis: The Queen Maud Block, Nunavut - Genesis of a large felsic igneous province in the earliest Paleoproterozoic and implications for Laurentian geotectonic models

Degree: Master of Science

Year this Degree Granted: 2007

_____

Signature

Abstract

New geochemical and Sm-Nd and U-Pb isotope data indicate the Queen Maud Block (QMB) is Paleoproterozoic in age and central to understanding assembly of northwestern Laurentia. Data indicate: 1) Felsic and subordinate mafic magmatism at 2.46-2.50 Ga. Ponding of mafic magmas below induced high-temperature partial melting of refractory lower-crust. 2) A 2.48-2.39 Ga sedimentary belt, the Sherman basin, dominated by 2.45-2.50 Ga detritus. 3) Regional 2.39 Ga granulite-grade metamorphism, with no evidence of tectonomagmatic activity concurrent with orogenesis in the adjacent Taltson-Thelon belt at 1.9-2.0 Ga. I propose the QMB was an incipient continental rift at ~2.5 Ga. Exhumation of 2.46-2.50 Ga granitoids produced in early stages of rifting provided detritus to a basin that underwent granulite-grade metamorphism at 2.39 Ga. The switch from extension to compression environments could be a result of Slave-Churchill collision at 2.39 Ga or far-field triggers affecting an intracontinental environment within a contiguous Slave-Churchill craton.

Acknowledgements

The Natural Sciences and Engineering Research Council (NSERC) of Canada financially supported this thesis through Discovery operating grants to Thomas Chacko (University of Alberta) and Larry Heaman (University of Alberta). Additional funding was provided by the Department of Earth and Atmospheric Sciences through Graduate Teaching Assistantships. Field support was provided by the Canada – Nunavut – Geoscience – Office.

I would like to thank Thomas Chacko and Larry Heaman for considerable guidance and support throughout the thesis. What was a great opportunity before we began grew into an amazing research project and I credit my advisors for allowing me to realize this. Without their input into this project the Queen Maud Block would remain as elusive as it once was. I would also like to thank Antonio Simonetti for assisting me, with great patience, in acquisition of all the *in-situ* geochronological data used in this study. I would like to thank Rob Creaser for aquiring all the Sm-Nd isotopic analyses used in this study, information critical in developing the petrogenetic model for this area. Also thanks to Don Resultay for sample preparation, and to Judy Fjoser for help during my terms as ATLAS Seminar Organizer.

A special thanks to my sister Karen, who showed nothing but unwavering faith, love, patience and support throughout my degree. Her encouragement allowed me to accomplish great things and I will strive to be a little bit like her everyday. And big love to the rest of my family, they have always believed in me, my father and mother and sister Jennifer.

Finally, many thanks to friends and colleagues who provided personal and professional support throughout my degree. I've grown as a person with the help of Hilary Corlett, Taras Nahnybida, Larry Amskold, Trevor MacHattie and countless others. Thanks to all.

Table of Contents

List of Tables

List of Figures

1. Introduction

The tectonomagmatic events that occurred in the earliest Paleoproterozoic (ca. 2.4-2.5 Ga) are well known globally, and are used both as indicators of continental rifting (Amelin et al., 1995; Aspler and Chiarenzelli, 1998) and as piercing points for continental reconstructions (c.f. Heaman, 1997; Dahl et al., 2006). Locally, such as in the Karelia craton, large volumes of these mafic igneous rocks have been preserved in the form of flood basalts and shallow-level layered intrusions (Amelin et al., 1995). More commonly, however, erosion has removed the near surface rocks, and evidence for this tectonomagmatic activity is preserved in mafic dyke swarms (e.g., Hearst, Matachewan, Mistissini, and Kaminak swarms), lower crustal xenoliths (e.g., Moser and Heaman, 1997), and in sedimentary basins (e.g., Huronian, Hurwitz and Snowy Pass basins) formed as a consequence of rifting. Recognition of these features in several parts of Laurentia and in Baltica leads some authors to propose that the earliest Paleoproterozoic represents the initiation of supercontinent breakup. For example, one proposal used the presence of both mafic magmatism, and unique Paleoproterozoic sedimentary sequences to suggest breakup of the Superior, Wyoming and Karelia cratons at 2.45 Ga. (Heaman, 1997; Roscoe and Card). Another model uses the widespread occurrence of 2.5 to 2.1 Ga intracontinental and passive margin sedimentary sequences to suggest that the entirety of northern Laurentia was assembled in the Archean and began breakup at ca. 2.5 Ga. (Aspler and Chiarenzelli, 1998).

Given the intrusion of voluminous mafic magmas into Laurentian crust at 2.4 to 2.5 Ga, it is somewhat surprising that granitoid rocks of this age are comparatively rare. Felsic to intermediate composition magmatic rocks crystallized in this time interval have been reported from the Superior, Wyoming and Sask cratons but occupy less than a few hundred square kilometers in each case (Krogh, 1996; Ashton et al., 1999; Chamberlain et al., 2003; Rayner et al., 2005). Recently, however, Schultz et al. (2007) documented a much more extensive exposure (at least 5000 km^2) of 2.46 to 2.50 Ga granitoid rocks from the Queen Maud block (QMB) of northwestern Laurentia (Fig. 1). In the northeastern and north-central QMB, intrusion of granitoids was followed closely by the formation of a sedimentary basin, the Sherman basin, which received the majority of its

detritus from 2.45 to 2.50 Ga source rocks. The Sherman basin was short-lived as sediments within the basin were buried and underwent granulite-facies metamorphism at ca. 2.39 Ga during the so-called Arrowsmith orogeny, which affected a large portion of northwestern Laurentia at this time (Bostock and van Breeman, 1994; Berman et al., 2005; Hartlaub et al., 2007).

Schultz et al. (2007) suggested two possible tectonic settings in which the QMB granitoids and closely associated Sherman basin may have formed: (1) an arc/back-arc setting, and (2) an incipient continent rift setting. For a number of reasons, a rift model was favoured but it was noted that bimodal mafic-felsic magmatism, a characteristic of many continental rifts, had not yet been documented in the QMB. In the present contribution, the nature of earliest Paleoproterozoic magmatism in the QMB in the context of Neoarchean magmatism in adjacent areas is further evaluated. Specifically, the geochronological and Sm-Nd isotope database for the QMB is supplemented with 4 additional U-Pb zircon dates on granitoid rocks, 3 new dates on mafic rocks and 15 additional Sm-Nd isotopic analyses on both granitoids and mafic rocks. Petrogenesis of both the granitoid and mafic rocks in light of major-, trace-element and Nd isotope data is also examined. Using these data, the tectonic model for the QMB is refined and considered are the broader implications of this model for the tectonic evolution of western Laurentia in late Neoarchean to earliest Paleoproterozoic time.

2. Western Churchill Province Regional Setting

The Churchill province west of Hudson Bay is bound to the northwest by the 2.0-1.9 Ga Taltson-Thelon Magmatic Zone and to the southeast by the 1.9-1.8 Ga Trans-Hudson Orogen (Fig. 1). Historically this province was distinguished from surrounding Archean provinces by distinctive Paleoproterozoic K-Ar ages (Stockwell, 1982) and has since been divided along the Snowbird Tectonic Zone into the Rae and Hearne domains (Hoffman, 1988; Hanmer, 2004), with the QMB located on the northwestern margin of the Rae domain (Fig. 1). The nature of the Snowbird Tectonic Zone is still contested (c.f. Sanborn-Barrie et al., 2001; Mahan and Williams, 2005) with regards to the significance and degree of Proterozoic re-working, but the Rae and Hearne are generally considered to

have become a coherent unit in the Paleoproterozoic (c.f. Mahan and Williams, 2005). Two sedimentary basins within the western Churchill province, initiated at ca. 2.45 Ga, contain the Hurwitz and Amer Groups (Aspler and Chiarenzelli, 1998).

2.1 Rae Domain Geology

Rocks of the Rae domain consist largely of 2.73-2.68 Ga supracrustal belts containing komatiite, basalt and quartzite assemblages (Skulski et al., 2003) intruded by 2.6 to 2.7 Ga granitoid plutons. Supracrustal belts in the northeastern Rae domain such as the Prince Albert Group contain 2.73 Ga juvenile mafic rocks that give little indication of interaction with older crust (MacHattie et al., 2007; Young et al., 2007). Similarly, depleted mantle Nd model ages (T_{DM}) obtained from 2.7 to 2.6 Ga plutonic rocks in the north-central Rae and the northeastern and central QMB indicate derivation of magmas from Neoarchean source rocks (Skulski et al., 2003; Schultz et al., 2007). The only evidence for more ancient rocks in the Rae domain comes from the southern QMB, where undated granitoids yield distinctly older T_{DM} ages between 3.3-3.9 Ga (Theriault et al., 1994), and from the southwestern Rae margin where model ages as old as 3.3 Ga have been reported (Hartlaub et al., 2005). Neoarchean plutonism (2.62 to 2.58 Ga) is ubiquitous in the Rae domain, subsequent to which ca. 1.85 to 1.81 Ga granitoid plutonism occurs and is temporally linked to Trans-Hudson magmatism (Peterson et al., 2002). Metamorphism and deformation in the northern Rae domain at ca. 2.35 Ga has only recently been documented (Berman et al., 2005). This event is better documented in the southern Rae domain where ca. 2.3-2.4 Ga metamorphism and plutonism has been attributed to subduction and collision related processes (Bostock van Breemen, 1994; Hartlaub et al., 2007).

2.2 Queen Maud Block Geology

Helicopter reconnaissance mapping conducted in the early 1960's (Heywood, 1961; Fraser, 1964, 1978) determined that the QMB largely comprises quartzofeldspathic gneisses, granitoids of various compositions and both metavolcanic and metasedimentary rocks. Further subdivision of the QMB was proposed by Schultz et al. (2007) based on

publicly available aeromagnetic data (Geological Survey of Canada, 2006). These data outline three north- to northeast-trending domains; a linear eastern magnetic high containing a lozenge shaped complex magnetic high (red through white colours straddling proposed QMB boundary in Fig. 2), a central magnetic low (blue in Fig. 2), and an internally complex western magnetic high (west of blue in Fig. 2). Recent fieldwork conducted in the area for this study demonstrates that magnetic high domains are dominated by moderately to strongly deformed quartz diorite and tonalite to granodiorite. Most of the QMB granitoids contain a significant amount of mafic minerals, such as biotite and hornblende, and are commonly orthopyroxene-bearing. The central magnetic low largely comprises migmatized pelites and semi-pelites characterized by anastomosing garnet-bearing leucosomes. Metasedimentary rocks are locally intercalated with mafic rocks of possible metavolcanic origin. Collectively, the metasedimentary and metavolcanic rocks of the central magnetic low are referred to as the Sherman Group supracrustals (Schultz et al., 2007). Both the Sherman Group supracrustals as well as the granitoids of the QMB exhibit a dominantly N-NE striking foliation with moderate to steep easterly dips. The occurrence of the garnet – cordierite – potassium feldspar assemblage in pelitic rocks and two-pyroxene assemblage in mafic rocks indicates that the eastern and central QMB was metamorphosed to granulite-facies conditions. U-Pb isotopic analysis of monazite in pelitic rocks indicates that granulite metamorphism occurred at ca. 2.39 Ga (Fig. 2; Schultz et al., 2007).

3. Igneous Rocks

There are three groups of igneous rocks exposed within the QMB and Rae domain. The two major groups are the QMB and Rae granitoids, which are distinguished on the basis of geochronology, geochemistry and spatial relationships. QMB granitoids occur exclusively west of the proposed Rae-QMB boundary (Fig. 2) and have igneous crystallization ages of 2.46 to 2.50 Ga (Schultz et al., 2007, this study). Rae granitoids occur both within the QMB and east of the proposed boundary and yield Archean crystallization ages from 2.6 to 2.7 Ga. Mafic rocks identified in the QMB comprise the third group and include a mafic xenolith within granite, an inferred mafic volcanic rock interlayered with Sherman Group supracrustals, and three mafic dykes. Samples were

collected from each of these three groups of rocks for further petrographic, geochemical and isotopic study. Sample locations are shown in map form in Figure 2. UTM coordinates of sample locations are given in Appendix 3.

3.1 Rae Granitoids

In the normative equivalent of the International Union of Geological Sciences classification scheme (Streckeisen and LeMaitre, 1979), the Rae granitoids range from quartz diorite to syenogranite with the majority of samples being granodiorite and monzogranite (Fig. 3). All granitoids are moderately to strongly deformed and variable altered, commonly containing secondary chlorite, epidote and sericite. The Rae granitoids are generally non-magnetic with the obvious exception being some rocks from the eastern magnetic high (Fig. 2).

Biotite ± hornblende quartz diorite, quartz monzodiorite and granodiorite make up 7 of 16 of the rocks collected from the Rae domain. Potassium feldspar porphyritic to megacrystic phases are common. Mafic minerals generally make up about 10% of the modal mineralogy but can be as high as 20 modal %. Within this group titanite, epidote and allanite occur as accessory phases. In many cases, epidote appears to be of magmatic origin with cores of allanite.

Two-mica biotite ± muscovite granodiorite to syenogranite, commonly with potassium feldspar phenocrysts and megacrysts make up the remaining 9 samples from the Rae domain. These rocks are generally more leucocratic than the quartz diorite to granodiorite suite. Accessory phases are less abundant. Epidote occurs in trace amounts and is likely a secondary mineral. One of the Rae granitoids, ST-1a, dated by Schultz et al. (2007) belongs to this group and yielded an age of 2636 ± 11 Ma. This is the only Archean rock that has been identified by geochronology west of the QMB boundary. Sample NT-5 also occurs west the of the QMB boundary. It is a leucocratic biotite – hornblende monzogranite, markedly more altered than other QMB samples, and interpreted to represent a Rae granitoid based on similar trace-element chemistry to ST-1a (discussed below).

3.2 QMB Granitoids

QMB granitoids, which are commonly magnetic, range from quartz diorite to monzogranite with the majority of samples falling into the tonalite and granodiorite fields (Fig. 3). Mafic minerals generally make up 10–15% of the modal mineralogy and comprise biotite-hornblende-orthopyroxene ± clinopyroxene. Seven of the thirteen QMB granitoid samples collected are orthopyroxene-bearing and thus could be termed charnockites or enderbites. Two of the samples (NT-7 and NT-7a) are garnet-bearing. Zircon and apatite are common and in some cases relatively abundant accessory minerals. The QMB granitoids are moderately to strongly deformed, with some samples exhibiting partial recrystallization of quartz and feldspar to granoblastic textures.

3.3 Mafic Rocks

Five mafic samples from the QMB were collected for this study (Fig. 2). All samples have sub-alkaline tholeiitic basalt compositions but have undergone varying degrees of metamorphism. One sample occurs as a mafic granulite xenolith within granitoid ST-6a and one occurs as a layer within pelitic metasedimentary rocks (NT-8a). The remaining three samples (NT-3, ST-1 and ST-2b) are interpreted to be mafic dykes; one of these, NT-3, is brecciated (Fig. 5a).

Xenolith ST-6a is a fine- to medium-grained, two-pyroxene mafic granulite, with ~60% plagioclase, ~40% combined mafic minerals including roughly equal proportions of clinopyroxene and orthopyroxene (25%), and equal proportions hornblende and opaque minerals (15%). Granoblastic texture is well developed within the feldspar and the sample contains up to 2% accessory rutile, as well as trace zircon. This and other xenoliths occur as oblate bodies no larger than 20 cm, and have sharp margins. NT-8 is an amphibolite interlayered with pelitic and semi-pelitic metasedimentary rocks. It likely represents a mafic lava flow, mafic sill or proximally derived mafic sediment. NT-8a is fine-grained, in part a result of deformation induced grain size reduction. The sample is extensively altered with pyroxenes largely converted to secondary amphibole. There is up to 5% sulphides and accessory phases include trace zircon and secondary biotite.

ST-1, ST-2b and NT-3 are fine- to medium-grained with variably developed granoblastic texture in the feldspar and mafic minerals. ST-1 and NT-3 are amphibolites, whereas ST-2b is a two-pyroxene mafic granulite. Mafic dyke ST-1 has a minimum width of ~50 m and an inferred northerly strike, paralleling a nearby linear lake. The rock is medium-grained and is now composed largely of secondary amphibole with minor biotite. ST-1 contains up to 60% combined mafic minerals, 5-6% opaque minerals, and abundant apatite and zircon. There is evidence of a primary mineral assemblage containing clinopyroxene but the mafic minerals are almost entirely altered to secondary amphibole. Mafic dyke ST-2b has a minimum width of ~30 m and an assumed northerly strike. ST-2b is highly recrystallized and contains ~75% combined mafics with roughly equal proportions orthopyroxene and clinopyroxene, up to 10% secondary amphibole, <5% sulphides, and trace secondary biotite. NT-3 contains ~50% combined mafic minerals, predominantly secondary amphibole, with ~5% clinopyroxene and trace orthopyroxene still visible. Accessory phases include secondary biotite and trace zircon.

4. Geochronology

Schultz et al. (2007) defined the eastern boundary of the QMB as the furthest easterly expression of 2.46 to 2.50 Ga magmatism, but noted that this observation did not preclude the presence of Archean rocks within the QMB. In order to constrain further the amount of Archean rocks in the QMB and the scale at which Archean- and QMB-aged granitoids were juxtaposed, 3 outcrops (ST-1, NT-3 and NT-7) containing multiple granitoid phases were targeted for additional geochronological study. A granitoid from one other site (ST-5) was also targeted to improve geochronological characterization of the western magnetic high. The prediction of the rift model that some of the mafic magmatism in the QMB should be similar in age to granitoid magmatism was also tested by analysis of 4 mafic samples. Previous age determinations (Schultz et al., 2007) along with new geochronology from this study are summarized in Figure 2 and Table 1. Concordia plots and electron backscatter images of selected grains from the granitoid and mafic samples are presented in Figures 4 and 5. Full U-Pb isotope analyses are given in Appendix 2.

The four granitoid samples and four mafic samples were investigated using the *in-situ* laser ablation - multi-collector - inductively coupled plasma - mass spectrometry (LA-MC-ICP-MS) technique (Simonetti et al., 2006) at the Radiogenic Isotope Facility, University of Alberta. This technique allows for analysis of zircon and monazite identified in conventional petrographic thin section and has been used as the primary geochronological tool for investigations in the QMB (Schultz et al., 2007). The NuPlasma MC-ICP-MS utilized for this technique is equipped with a unique collector array that allows for simultaneous acquisition of ion signals from ^{203}Tl through ^{238}U. Laser ablation is performed using an Nd:YAG UP 213nm laser system (New Wave Research), and data acquisition consists of 1 second integrations over 30 seconds, typically using a laser beam diameter of 30 μm and an ablation depth of <15 μm. An in-house zircon standard (LH-94-15: Ashton et al., 1999) was used for all geochronological investigations of felsic igneous rocks and detrital samples in both this study and Schultz et al. (2007). An international zircon standard (BR266; Stern and Amelin, 2003) was used for geochronological investigation of mafic igneous rocks in this study for more consistent normalization of Th/U ratios. Th/U ratios were obtained during routine runs for U-Pb geochronology by aligning the ^{232}Th ion signal with those for U and Pb. Isotopic ratios for the LA-MC-ICP-MS technique are reported at 3% (2 sigma) $^{207}Pb/^{235}U$, $^{206}Pb/^{238}U$ and 1% $^{207}Pb/^{206}Pb$ external reproducibility. Mafic dyke NT-3 was also investigated using the isotope dilution – thermal ionization mass spectrometry (ID-TIMS) technique. For ID-TIMS analyses zircons were isolated using standard crushing and mineral separation techniques. Multi-grain zircon fractions were dissolved and U and Pb were isolated and purified using anion exchange chromatography. U and Pb aliquots were loaded together onto Re filaments and isotopic compositions were determined on a VG354 mass spectrometer. Details of the U-Pb zircon ID-TIMS technique at the University of Alberta are outlined in Heaman et al. (2002). Concordia plots and age calculations (LA-MC-ICP-MS and ID-TIMS) were determined using Isoplot Version 3.0 (Ludwig, 2003). Error ellipses and quoted ages are at the 2 sigma level of uncertainty. Many of the zircons in the granitoids display oscillatory zoning, which is likely of igneous origin. All ages for granitoids are therefore interpreted to be that of igneous

crystallization. The paragenesis of zircon grains in the mafic rocks is less certain but, as discussed further below, most of the analyzed grains are inferred to be of igneous origin.

4.1 Granitoid Geochronology

Sample ST-1b from the eastern magnetic high is a coarse-grained to megacrystic hornblende-biotite tonalite. A total of 17 U-Pb analyses were obtained on 10 zircon grains. Two analyses yielding younger ages and two analyses yielding slightly older ages are outliers to the primary age grouping and were not included in the age calculation. 13 analyses on 8 zircons cluster on or near concordia and yield a weighted mean (WM) $^{207}Pb/^{206}Pb$ age of 2469 ± 8 Ma (Fig. 4a; backscatter image of grain 14). Sample ST-1a, another granitoid from this same location, yielded an Archean age of 2636 ± 11 Ma (Schultz et al., 2007).

Sample ST-5a is a gneissic hornblende-biotite-orthopyroxene tonalite from the western magnetic high. Nine analyses were obtained on 5 grains. Three of these analyses gave distinctly younger ages and were not included in the age calculations. The remaining 6 analyses on 4 grains are still fairly complicated with two near concordant, slightly younger analyses and 4 near concordant, slightly older analyses. Several different treatments of the data yielded similar results and given the proximity of these data to the concordia curve, the WM $^{207}Pb/^{206}Pb$ age of 2470 ± 14 Ma (Fig. 4b; backscatter image of grain 2) is the best estimate of the crystallization age of this granitoid.

Sample NT-3c from the eastern magnetic high is a coarse-grained to megacrystic biotite-hornblende-orthopyroxene ± clinopyroxene granodiorite. Eight analyses on 6 grains were obtained. One discordant analysis yielding the same $^{207}Pb/^{206}Pb$ age within error was not included in the age calculation of this otherwise very concordant group of analyses. Seven analyses on 5 zircons cluster on or near concordia and yield a WM $^{207}Pb/^{206}Pb$ age of 2502 ± 7 Ma (Fig. 4c; backscatter image of grain 3). Sample NT-3a, a biotite-hornblende granodiorite from this location yielded an age of 2490 ± 29 Ma (Schultz et al., 2007), which, within analytical uncertainty, is identical of the age reported here for the pyroxene-bearing granodiorite.

Sample NT-7a is a coarse-grained biotite-garnet granodiorite from the central magnetic low. A total of 17 U-Pb analyses were determined on 9 zircon grains. Four younger analyses and one slightly older analysis are outliers to the primary age group and were not included in age calculations. Twelve analyses on 8 zircons ranged from concordant to 13% discordant and a linear regression treatment yielded an upper-intercept age of 2496 ± 13 Ma (Fig. 4d; backscatter image of grain 10) that is identical within error to a WM $^{207}Pb/^{206}Pb$ age calculated with 1 of 12 analyses rejected. The young lower intercept age indicates only recent isotopic disturbance of these grains. This is identical to the other granitoid phase at this location (NT-7) that yielded an age of 2497 ± 19 Ma (Schultz et al., 2007).

A striking feature of the U-Pb zircon data for QMB granitoids is that out of more than 75 analyses on 51 zircon grains in 8 samples, there is no indication of the presence of inherited zircons significantly older than the inferred crystallization ages of these granitoids. This suggests either that there was little or no zircon remaining in the source regions of the QMB granitoids or that older zircon were completely dissolved in the granitoid magmas.

4.2 Mafic Rock Geochronology

The zircons identified in thin section of the mafic rocks ranged from small, subhedral grains in ST-6a, NT-8a to larger, anhedral to subhedral, grains up to 100 μm in length in ST-1, and one very large single grain in NT-3. None of the grains exhibited fine-scale oscillatory zonation, although visible zoning patterns were observed in single zircons in NT-3 and ST-1 (Fig. 5c). Samples ST-6a, NT-8a, NT-3 and ST-1 were investigated using the *in-situ* LA-MC-ICPMS method, while sample NT-3 was also investigated using ID-TIMS.

Dyke NT-3 had little outcrop exposure and occurs as brecciated blocks within a granitoid (Fig. 5a). Zircon mineral separates selected for ID-TIMS analysis were colourless, irregular fragments. A composite fraction of 10 zircon fragments had a Th/U ratio of 0.83, a moderate U content of 215 ppm and yielded a near-concordant $^{207}Pb/^{206}Pb$ age of 2483.1 ± 1.4 Ma (Fig 5b). Seven of 8 LA-MC-ICPMS analyses on a single grain yielded

an age of 2509 ± 9 Ma (Fig 5b). The one zircon that was analyzed *in situ* was very large for a fine-grained mafic rock, ~350 x 200μm, and contained within a clot of coarser pyroxene rimmed by biotite. It could represent a slightly older xenocrystic zircon within a small xenolith or a primary magmatic zircon that underwent some reaction during fluid influx or a later heating event. The implications are that if the single grain analyzed by LA-MC-ICPMS is considered primary, the grain fragments analyzed by ID-TIMS could represent metamorphic zircon growth during intrusion of the QMB granitoids. However, the morphology of the grain fragments analyzed by ID-TIMS suggest they came from similarly large grains crushed during mineral processing and not smaller anhedral grains indicative of metamorphic growth. If the single grain analyzed is a slightly older xenocryst, one can consider the ID-TIMS age that of igneous crystallization, an interpretation that corresponds well with the fairly high Th/U ratio (Hoskin and Black, 2000; Hoskin and Schaltegger, 2003). Considering the age of other mafic rocks and granitoids within the QMB the ID-TIMS age of 2483.1 ± 1.4 Ma is our best estimate for the age of igneous crystallization.

Mafic sample ST-1 contains abundant zircon in thin section with grains ranging in size from 50 to 250 μm. Most grains show little to no internal structure on backscatter electron images. One grain fragment exhibits a linear zoning pattern with relatively broad zones parallel to the length of crystal (grain 4; Fig. 5c). The zoning pattern broadly resembles that described by Hoskin (2000) for zircon from the diorite phase of a compositionally zoned I-type pluton. Hoskin suggested that the lower viscosity of mafic magmas inhibits the development of fine-scale oscillatory zoning and leads to broader-scale compositional zoning such as observed in grain 4. Seventeen analyses on 7 different zircon grains from sample ST-1 yielded Th/U ratios between 0.46 and 1.07. Although not definitive, the relatively high Th/U ratio of these zircon grains is more characteristic of igneous than metamorphic zircon (Hoskin and Black, 2000; Hoskin and Schaltegger, 2003). Furthermore, all of the grains analyzed in this sample occur within plagioclase grains or along grain boundaries adjacent to plagioclase, lessening the possibility that breakdown of Zr-bearing mafic phases of igneous (i.e. pyroxene) or metamorphic (i.e. hornblende) origin could have contributed to the growth of metamorphic zircon (Fraser et

al., 1997). The analyses yielded a range of near concordant ages from 2380 to 2520 Ma with the predominant grouping from 2440 to 2500 Ma. There is no correlation between Th/U ratios and the younger age grouping, indicating there is no evidence for the existence of low Th/U metamorphic zircon growth. Therefore, the younger grains likely experienced lead loss during ca. 2.39 Ga metamorphism. A WM $^{207}Pb/^{206}Pb$ age of 13 analyses (excluding the four youngest analyses) gives an age of 2475 ± 15 Ma (MSWD = 5.3; Fig. 5c). A WM $^{207}Pb/^{206}Pb$ age of 9 analyses (excluding the 2 youngest and 2 oldest analyses from the primary grouping) yielded an age of 2475 ± 8 Ma (MSWD = 0.68). I consider the 2475 ± 15 Ma age to be the best estimate of the crystallization age of this mafic magma.

Three small zircons were identified in sample NT-8a. They occur within both plagioclase and metamorphic hornblende, on which only one laser analysis each could be performed. The Th/U ratios ranged from 0.19 to 0.29, which could suggest a metamorphic origin for the grains. Two analyses fall on a similar discordia line and when freely regressed yield an age of 2467 ± 17 Ma or when anchored to a zero age lower intercept yield and age of 2486 ± 13 Ma (Fig 5d). A WM $^{207}Pb/^{206}Pb$ age of the three analyses yields an age 2479 ± 39 Ma, similar to the anchored regression through three points. Given the similarity to ages from other mafic samples having zircon Th/U ratios more indicative of a magmatic origin, a maximum age of ca. 2480 Ma is considered that of igneous crystallization and is within the range of QMB magmatism.

Only two very small zircons were identified in the thin section from mafic xenolith ST-6a. Both have low Th/U ratios of 0.33 and 0.38. Analyses of these zircons yielded discordant data that regardless of treatment yield a ca. 2420 Ma age. Although the granitoid at location ST-6 hosting the mafic xenolith is one of the few for which no age data have been obtained, by analogy with other QMB granitoids, it is unlikely to be younger than 2420 Ma. Given the similarity in Th/U ratios of zircon grains in sample ST-6a and NT-8a, where an igneous origin for the zircon was favoured, these likely do not represent pure metamorphic growth but rather a U-Pb system that has been partially reset.

The 2420 Ma date may represent a mixed age between igneous crystallization and ca. 2.39 Ga metamorphism.

5. Geochemistry

Thirty-four samples of igneous rocks from the QMB and adjacent Rae domain were analyzed for major-, trace- and rare-earth element compositions at Activation Laboratories in Ancaster, Ontario. This included twenty-nine granitoid samples, and five mafic samples. Major elements and Sc, Be were determined by fusion ICP and all other elements by ICP-MS. Analytical errors for the data based on analyses of reference materials are routinely accurate to better than 5% relative of the measured value for fusion ICP with the exception of K_2O and P_2O_5 which are accurate to <10% relative. ICP-MS analyses were commonly accurate to <10%, except where concentrations approached detection limits, accuracy decreased. Representative whole-rock analyses and averages of all samples for the QMB and Rae domain granitoids and QMB mafic rocks are given in Table 2. Complete major- and trace-element data for all samples are given in Appendix 2.

5.1 Major-element Composition of Rae and QMB Granitoids

The major-element data reveal a number of systematic differences between the Rae and QMB granitoid suites. The majority of Rae granitoids have between 65 and 75 wt.% SiO_2 whereas most QMB granitoids have between 59 and 68 wt.% SiO_2. Similarly, there is an overall difference between the suites in their degree of alumina saturation with the majority of Rae granitoids being weakly to moderately peraluminous in contrast to QMB granitoids, which are predominantly weakly peraluminous to metaluminous (Fig. 6). One QMB granitoid, (NT-7), is moderately peraluminous. Harker variation diagrams (Fig. 7) show overall enrichment of QMB granitoids relative to Rae granitoids in FeO, MgO, TiO_2 and P_2O_5. A distinction between the granitoid groups can also be seen in the Mg number (molecular $MgO/(MgO + FeO_{total})$ where Rae granitoids have uniform Mg numbers of about 0.45 and QMB granitoids vary between 0.2 and 0.5

5.2 Trace-element Composition of Rae and QMB Granitoids

Of the twenty-nine granitoid samples analyzed, 14 were collected east of the QMB boundary and are considered Rae granitoids. Of samples collected west of the QMB

boundary, 13 exhibit similar REE profile patterns and are considered QMB granitoids. Two samples, ST-1a and NT-5, were collected west of the boundary but are considered Rae granitoids (discussed below). The trace-element profiles of the primary QMB and Rae granitoid groups are shown in Figure 8 a through d, and all trace-element data, including trace-element ratios, discussed in the text are normalized to primitive mantle (PM; McDonough and Sun, 1995).

Rae granitoids (Fig. 8a) are enriched in light (LREE) relative to heavy (HREE) rare earth elements with La/Yb ratios ranging from 17 to 49 (Fig. 9), averaging 32 and Gd/Yb ratios averaging 3.3. The profile is characterized by strong negative Nb and Ti anomalies and a weak to moderate negative Y anomaly. LREE enrichment is ~10 to 100 times PM and HREE enrichment is 1 to 4 times PM. Th/Nb ratios vary from 10 to 22 and average 15 with the exception of BT–4 and –3 which have ratios of ~6 (Fig.9). Samples ST-1a and NT-5, although located west of the QMB boundary, have trace-element patterns similar to those of the Rae granitoids (Fig. 8b). In the case of sample ST-1a, geochronological data (Schultz et al., 2007) indicate that this is in fact an Archean granitoid (2635 ± 11 Ma) and therefore should be considered with the other Rae granitoids. On the basis of the similarity in trace-element patterns and enhanced alteration of minerals in sample NT-5, it is inferred that it is also an Archean granitoid located within the QMB. Samples ST-1a and NT-5 have exaggerated Th/Nb and La/Yb ratios relative to the rest of the Rae domain granitoids. For this reason these samples are not included in averages of geochemical data for Rae domain rocks, although if included only serve to heighten the difference between trace-element ratios for Rae domain and QMB granitoids.

QMB granitoids (Fig. 8a,b) are less LREE enriched and more HREE enriched than the Rae granitoids. This results in lower La/Yb ratios ranging from 7 to 35 (Fig. 9), averaging 16 and Gd/Yb ratios averaging 2.5. The pattern is characterized by strong negative Ti anomaly and flat to moderate negative Y anomaly. There is also greater variability in Zr and Hf contents with a few samples having Nd/Zr > 1. The most pronounced difference between the QMB and Rae granitoid suites is in their Th/Nb ratios; the QMB granitoids have low Th/Nb ratios ranging from 0.2 to 5.8 and averaging 2.3 in contrast to the Rae

granitoids which have an average Th/Nb of 14 (Fig. 9). This large difference primarily reflects the low Th content of the QMB granitoids

5.3 Major-element Composition of QMB Mafic Rocks

The mafic rocks identified in the QMB comprise the 5 samples described above. These rocks are basaltic in composition and contain between 46 to 50 wt.% SiO_2, 11 to 15 wt.% Al_2O_3 and 0.2 to 1.4 wt.% K_2O. FeO_T contents are consistent at 14 to 15 wt.% with the exception of NT-3, which contains only 9 wt.% FeO_T. Three of the samples (ST-1, ST-6a, NT-8a) have high TiO_2 (> 2 wt. %) and one sample (ST-1) also has high phosphorus content. Mg numbers range from 0.62 to 0.32 indicating that none of these rocks represent primary mantle melts (Mg number ~ 0.75) but reflect significant degrees of fractionation and/or crustal assimilation.

5.4 Trace-element Composition of QMB Mafic Rocks

The QMB mafic rocks, like the QMB granitoids, are generally characterized by low Th/Nb ratios (0.3 to 3.3 with four of five samples < 1). On the basis of their trace element profiles ST-6a, NT-8a and the dykes make up three different groups (Fig. 10). Dyke samples ST-2b and NT-3 (triangles; Fig. 10) all have very similar trace element profiles, LREE enrichment (La/Yb = 6.4 and 4.2), and Th < Nb < La. ST-1 (diamonds; Fig. 10) has a similar trace element profile but is substantially more enriched in LREE (La/Yb = 14.1) in comparison to ST-2b and NT-3. All three samples contain a moderate negative Zr, Hf and Ti anomalies. The only marked difference in the profiles is the Th/Nb ratio where ST-1 and ST-2b exhibit Th/Nb ratios of < 1, NT-3 has Th > Nb and a slightly enriched LREE pattern relative to ST-2b. NT-8a and ST-6a (squares; Fig. 10) are identical and have nearly flat REE profiles (La/Yb ≤ 3), Th < Nb ≈ La, and enriched ~ 11 times the PM. The Zr, Hf and Ti negative anomalies are weak to flat and these samples are also characterized by Th/Nb ratios of less than one.

6. Sm-Nd Isotope Geochemistry

In addition to Sm-Nd isotope data presented in Schultz et al. (2007), several more samples were analyzed in the present study, including all the mafic rocks collected in this study. All analyses were performed at the Radiogenic Isotope Facility at the University of

Alberta. Rock powders prepared for major- and trace-element analysis were weighed and spiked with known amounts of ^{149}Sm-^{150}Nd tracer, and then Sm and Nd were separated by conventional ion-chromatography techniques (Creaser et al., 1997) Solution mode Sm-Nd isotope analyses were performed on a NuPlasma MC-ICP-MS following procedures outlined in Schmidberger et al. (2002). For Nd isotopic acquisition, the analysis of unknown sample solutions was alternated with a 200 ppb solution of an in-house Nd Alfa isotopic standard solution (accepted $^{143}Nd/^{144}Nd$ = 0.512265 based on calibration to the La Jolla standard). In total 22 samples have been analyzed for their Sm-Nd isotopic composition, of which 7 are known or assumed Rae granitoids, 10 are known or assumed QMB granitoids, and 5 are QMB mafic rocks. ε_{Nd} values calculated at 2.48 Ga are summarized Figure 2, Table 1 and Figure 11. Full Sm-Nd isotope analyses are given in Table 3.

The 7 Rae granitoid samples analyzed have a relatively narrow range of T_{DM} ages from 2.8 to 3.1 Ga calculated using the depleted mantle curve of Goldstein et al. (1989). At the known or estimated time of their crystallization (~ 2.6 to 2.7 Ga), the ε_{Nd} values of these granitoids ranged from ~ -1 to +1 indicating derivation primarily from Neoarchean source rocks. At the time of QMB granitoid formation (ca. 2.48 Ga), these same Rae granitoids would have had ε_{Nd} values between –1.9 and –3.2.

The 10 QMB granitoids samples have T_{DM} ages from 2.9 to 3.1 Ga, nearly identical to those of the Rae granitoids. The ε_{Nd} values of QMB granitoids at the time of crystallization (ca. 2.48 Ga) define a narrow range between –1.5 to 0.0, with 7 of the 10 analyses clustering from –1.5 to –1.3. NT-3b, ST-2a and ST-7, among the more mafic QMB granitoid samples, have slightly more juvenile Nd isotope compositions. It should be noted that the ε_{Nd} (2.48 Ga) values of the Rae and QMB granitoids, although similar, are not identical. Specifically, the QMB granitoids define a slightly more juvenile range of values with no overlap of data between the two suites. This indicates that the QMB granitoids were derived from Neoarchean source rocks with a slightly higher Sm/Nd ratio than those that produced the Rae granitoids or that, in addition to crustal source rocks, a small proportion of juvenile mafic magmas were involved in QMB granitoid production.

The three mafic dykes within the QMB have similar T_{DM} ages from 2.9 to 3.0 Ga whereas the two other mafic samples have high $^{147}Sm/^{144}Nd$ ratios that do not permit a reliable estimate of model ages. The dykes have ε_{Nd} (2.48 Ga) similar to the QMB granitoids from –1.3 to +0.2, while the other mafic samples are more juvenile having values of +1.5 and +1.8. Given that the depleted mantle at 2.48 Ga has an estimated ε_{Nd} value of +4.5, this indicates that all the mafic samples reflect some degree of crustal contamination, assuming the original source for these magmas was the depleted mantle.

7. Discussion

Both this study and Schultz et al. (2007) describe a number of features that must be addressed when considering the genesis of the QMB:

1. Mafic rocks within the QMB including mafic dykes and inferred mafic volcanic rocks were emplaced at ca. 2.48 Ga, coeval with granitoid plutonism.
2. The overall character of ca. 2.48 Ga magmatism in the QMB is bimodal in terms of SiO_2 contents, with samples ranging from 46 to 50 and 59 to 68 wt.% SiO_2. No intermediate samples comprising 50 to 59 wt.% SiO_2 have been identified.
3. The common occurrence of orthopyroxene in QMB granitoids suggests a high-temperature origin for these magmas. This inference is consistent with the lack of identified xenocrystic Archean zircon detected in any of the U-Pb zircon analyses of QMB granitoids.
4. Felsic and mafic igneous rocks from the QMB and 2.6 to 2.7 Ga granitoids from the adjacent Rae domain span a wide range of crystallization ages and compositions, yet have a narrow range of T_{DM} ages from 2.8 to 3.1 Ga. This indicates derivation from or contamination by a Neoarchean crustal source region.
5. The ε_{Nd} (2.48 Ga) values of QMB granitoids range from –1.5 to 0.0 whereas Rae granitoids range from –3.2 to –1.9. This difference indicates QMB granitoids were derived from Neoarchean crustal source rocks with a slightly higher Sm/Nd ratio or that a small proportion of juvenile mafic magma was incorporated in the QMB granitoids.

6. Mafic rocks of the QMB have ε_{Nd} (2.48 Ga) values ranging from +1.8 to –1.3, in part overlapping the range of values obtained for QMB granitoids. This indicates that QMB mafic magmas, which were likely derived from a depleted mantle source, underwent varying degrees of crustal contamination.
7. The mafic rocks and granitoids of the QMB have low Th/Nb (0.2 – 5.8), a characteristic that distinguishes them from Rae granitoids which generally have Th/Nb $\geq$ 10.
8. Although both Rae and QMB granitoids exhibit LREE enrichment relative to primitive mantle, the REE profile of Rae granitoids is steeper (La/Yb ~32) than that of the QMB granitoids (La/Yb ~ 16).
9. A sedimentary basin, the Sherman basin, formed in the QMB concurrent with or soon after intrusion of the QMB granitoids (Schultz et al., 2007). The basin is dominated by 2.45 to 2.50 Ga detritus.
10. The QMB underwent granulite-grade metamorphism at ca. 2.39 Ga (Schultz et al., 2007).

7.1 Constraints on the Nature of the Source Region of QMB Granitoids

Prior to QMB magmatism, three tectonomagmatic events occurred within the northern Rae domain that affected the nature of the lower crust and in turn subsequent granitoid production. These events include: (1) early 2.8-3.1 Ga production or homogenization of crust reflected in regional T_{DM} ages of later magmatic rocks; (2) ca. 2.7 Ga mafic-ultramafic with subordinate felsic magmatism; and (3) voluminous ca. 2.6 Ga granitoid plutonism.

The first event is imaged by granitoids of the northern Rae domain and the QMB in that both granitoid suites have similar T_{DM} ages over a wide range of crystallization ages (Skulski et al., 2003; Schultz et al., 2007; this study). This suggests that most of this region was constructed on relatively homogeneous 2.8-3.1 Ga basement and subsequent granitoid plutonism continued to draw from crust of this age. The second major event is widespread ca. 2.7 Ga magmatism associated with formation of the majority of Archean granite-greenstone belts in the northern Rae domain (MacHattie et al., 2007; Young et al., 2007). Mafic to ultramafic magmas that ponded at ca. 2.7 Ga in the Rae lower crust

caused partial melting, which contaminated mafic magmas and erupted as rare intermediate to felsic magmas within the volcanic successions (Skulski et al., 2003). This process likely served to deplete the lower crust in incompatible major elements, LREE and Th. Similarly, extensive ca. 2.6 Ga granitoid plutonism would have further depleted the lower crust in these elements and produced a refractory lower crust in the northern Rae domain. Relatively high temperatures would be required in order for this crust to generate additional granitoid magma during later events.

An additional comment can be made about the similarity in trace-element profiles of Rae granitoids produced during ca. 2.7 and 2.6 Ga events. The salient features of these profiles, such as high Th/Nb (Nb trough), LREE enrichment and accompanying negative Nb and Ti anomalies (Fig. 8), would generally be attributed to a convergent margin setting (e.g. Pearce, 1982). Because these granitoids span at least two distinct accretionary events yielding crystallization ages spanning ca. 150 m.y., the similarities in T_{DM} ages and consistent geochemical signatures of Rae granitoids are likely a result of intracrustal recycling and the subduction-like trace-element signature of later magmatic events is inherited from initial crust formation (c.f. Morris et al., 2000). Thus, the trace-element compositions of the granitoids are not unambiguous indicators of tectonic environment any time after extraction from their depleted mantle source.

7.2 Origin of QMB Granitoids

The QMB granitoids comprise a mineralogically and geochemically distinctive suite relative to typical granitoids of the Rae domain. QMB granitoids are characterized by low Th/Nb, lower La/Yb, a less pronounced negative Y anomaly, and Zr and Hf enrichment relative to Rae granitoids (Fig. 8b,c). QMB granitoids are also generally more primitive than their Rae counterparts having a lower range in SiO_2 contents, and containing a greater proportion of mafic mineral phases, in particular, orthopyroxene. Finally, QMB granitoids are devoid of xenocrystic Archean zircon despite being derived from Neoarchean crustal source rocks.

All of these features are consistent with the QMB granitoids being high-temperature melts produced from a refractory lower crust. The QMB granitoids exhibit LREE and Th depletion relative to Rae granitoids as a result of extraction of Rae granitoids from the same source region. The most striking feature is the low Th concentrations of the QMB granitoids. The greater degree of Th relative to LREE depletion should be expected, as Th is more incompatible in partial melting processes than the other trace elements displayed in Figure 8 (Nash and Crecraft, 1985). Enrichment of HREE in QMB granitoids relative to Rae granitoids requires melting of mineral phases such as zircon with an affinity for HREE. The high concentration of Zr and Hf in the QMB granitoids suggests complete consumption of zircon during partial melting of the source region. The consumption of zircon during partial melting is also consistent with the lack of xenocrystic zircon in the QMB granitoids.

The QMB granitoids also represent a distinctive group in terms of Nd isotope geochemistry. Both the QMB and Rae granitoids display the same narrow T_{DM} age range from 2.8 to 3.1 Ga but diverge in their ε_{Nd} (2.48 Ga) values (Fig. 11), with QMB granitoids being more juvenile (–1.5 to 0.0) than the Rae granitoids (–3.2 to –1.9). This difference in ε_{Nd} values is again consistent with QMB granitoids being generated from a source that had experienced a prior episode of melt depletion. Specifically, extraction of LREE-enriched Rae granitoid magmas at ca. 2.7 and 2.6 Ga would have slightly increased the Sm/Nd ratio of the melt residue. As a consequence, partial melting of this melt-depleted lower crust at ca. 2.48 Ga would have produced granitoids with higher Sm/Nd and higher ε_{Nd} (2.48 Ga) values than that of the Rae granitoids.

The present data also provide some insight on the extent of mantle contribution to the QMB granitoids. The two most mafic QMB granitoid samples NT-3b and ST-7 and sample ST-2a have slightly more juvenile ε_{Nd} (2.48 Ga) values than most of the other QMB granitoid samples, –1.0, 0.0 and –0.6 respectively. This observation suggests that the mafic composition of these granitoids cannot simply reflect accumulation of mafic crystals derived from a more felsic, crustally-derived melt. Rather, these granitoids must have been derived from a distinct and isotopically more juvenile crustal source than the

remaining QMB granitoids or mixed to a limited degree with mantle-derived mafic magmas.

It should be noted, however, that mafic rocks from the QMB range from 46-50 wt.% SiO_2 and granitoids from 59-68 wt.% SiO_2; no intermediate rocks have been identified. This implies that very little of the granitoid production in the QMB is a result of direct differentiation from the basaltic melts or of extensive mixing between basaltic and granitic melts. Both these scenarios would have produced a full SiO_2 compositional spectrum as opposed to the observed bimodal felsic and mafic suites. This observation also suggests that the genetic link between QMB mafic rocks and granitoids is in large part indirect, with the QMB mafic magmas not contributing volumetrically to granitoid magmatism, but providing primarily heat.

7.3 Origin of QMB Mafic Rocks

The discovery in the present study of mafic igneous rocks of the same age as the QMB granitoids is critical in that it provides a mechanism whereby refractory lower crust could be heated sufficiently to produce granitoid magmas. Specifically, underplating of mafic magmas beneath Rae crust supplied the thermal impetus for partial melting of the lower crust. The origin of these mafic magmas is central to understanding the tectonic environment in which 2.46-2.50 Ga QMB magmatism occurred. Possible tectonic settings for the generation of the QMB mafic magmas include arc/back-arc and continental rift settings. Although only a few mafic rocks were investigated in this study, several geochemical and isotopic features of these rocks help to distinguish which of these two settings is more likely.

The ε_{Nd} (2.48 Ga) values of the QMB mafic rocks are as high as +1.8, which is relatively close to the ε_{Nd} value of the depleted mantle at that time (+4.5). Thus, primary QMB mafic magmas were probably derived from a depleted upper mantle source broadly similar to mantle that produces mid-ocean ridge basalts. Basaltic magmas with depleted mantle-like Nd isotope compositions can be produced in both rift and arc settings. The Th/Nb of basalts from the two settings is, however, distinctly different. The characteristic

Nb trough of arc basalt trace-element profiles results in elevated Th/Nb ratios, on average greater than 4. In contrast, the Th/Nb ratios of rift-related basalts are typically less than 2 (GEOROC database of igneous rock compositions; http://georoc.mpch-mainz.gwdg.de/georoc/Entry.html). As might be expected, back-arc basalts share some features of both arc and rift settings and therefore generally have intermediate Th/Nb ratios. With the exception of sample NT-3, which is discussed further below, the Th/Nb ratios of the other QMB mafic samples are all less than 1, a result that is more consistent with a rift rather than an arc or a back-arc setting. The higher Th/Nb ratio of sample NT-3 (Th/Nb = 3.3) is due to a relative Th enrichment (not Nb depletion), and therefore contamination with a Th-enriched mid-crust is a likely scenario. For example, mixing involving low Th/Nb sample ST-2b (~90 wt.%) and a crustal contaminant equivalent to the average composition of the Rae granitoids (~10 wt.%) analyzed from this study can replicate the incompatible trace element profile of sample NT-3. Importantly, this minor amount of contamination does not markedly change the REE profile or the major-element composition of the original, uncontaminated magma. In more general terms, crustal contamination can only increase the Th/Nb of primitive basaltic magmas. Thus, the low Th/Nb of the QMB mafic samples cannot be attributed to crustal contamination but must reflect a geochemical characteristic inherent to these magmas.

Another set of trace-element parameters that are useful in tectonic discrimination of basalts is Ti and V (Shervais, 1982). A comprehensive evaluation of various tectonic discrimination diagrams for basaltic rocks led Vermeesch (2006) to suggest that the simple bi-variate V-Ti plot is one of the most effective diagrams for distinguishing basalts produced in island arc, mid-ocean ridge and ocean-island settings.

As explained by Shervais (1982), the petrological basis of this diagram is that oxygen fugacity variations affect the mineral-melt partition coefficients of V but not of Ti. As a result, partial melting under oxidizing conditions of arc magma generation produces melts with low Ti/V compared to melts produced under more reducing conditions of mid-ocean ridge or ocean-island magma generation. Further, differentiation of magmas involving significant amounts of magnetite and/or hornblende crystallization, as

commonly occurs in continental arcs, produces different fractionation trends (decreasing V and Ti and slightly increasing Ti/V) than tholeiitic differentiation involving primarily olivine-pyroxene-plagioclase crystallization (increasing Ti, V and Ti/V).

Figure 12 is a V vs. Ti plot that compares the QMB mafic rocks with basalts from a variety of tectonic settings. Most of the data used were obtained from the large GEOROC database of igneous rock compositions (http://georoc.mpch-mainz.gwdg.de/georoc/Entry.html). The data for back-arc basalts were taken from the PetDB database (http://www.petdb.org/download_pg.jsp). I restricted comparison to rocks having between 45 to 55 wt.% SiO_2. Consistent with Vermeesch's (2006) conclusion, the V-Ti plot is effective in distinguishing between island arc (IAB) and mid-ocean ridge (MORB) basalts. Predictably, back-arc basalts extend across both the IAB and MORB fields. Continental margin arc analyses (e.g., Andean basalts) plot mainly in the MORB field but at lower V concentrations on average than IAB. This difference between island arc and continental arc signatures reflects magnetite and hornblende fractionation trends noted above.

The QMB mafic rocks plot almost exclusively in the MORB field, with only one sample plotting on the boundary between IAB and MORB fields. More importantly, three of five QMB mafic samples have both high Ti (>14,000 ppm) and high V (>350 ppm). Of the more than 1000 analyses of island arc, continental arc and back-arc basalts shown in this compilation, only four share that combination of characteristics. Thus, I would conclude that basalts enriched in both Ti and V are exceedingly uncommon in arc-related environments. The QMB data are more similar to data from continental flood and rift basalt provinces (e.g., Columbia River, Deccan and Mesoproterozoic U.S. Mid-Continent Rift basalts). In all cases, the data plot dominantly in the MORB field and contain a significant proportion of analyses with high Ti and V. The elevated Ti and V contents of these basalts can be explained by a tholeiitic fractionation trend (olivine-pyroxene-plagioclase crystallization) in which magnetite crystallization, and associated V and Ti depletion is suppressed by the reducing character of the magmas (Shervais, 1982).

Admittedly, the data available for QMB mafic rocks are limited and therefore the conclusions drawn above must be regarded as tentative. Nevertheless, I would argue that the combination of the bimodal character of QMB magmatism, low Th/Nb and high Ti and V contents of the mafic rocks are better explained by an incipient continental rift than an arc/back-arc setting.

7.4 Tectonic Environment

The proposal put forth by Schultz et al. (2007) defined the QMB as the site of an incipient continental rift whereby upwelling asthenosphere triggered melting of lower-crust and resulted in emplacement of 2.46 to 2.50 Ga QMB granitoids. Continued extension exposed these granitoids and allowed for them to become the primary source of detritus in the Sherman Basin. One of the shortcomings of this model was the lack of coeval mafic magmas indicative of a rift setting. This study presents evidence for the existence of both felsic and mafic magmas. These mafic rocks have a distinctive trace-element composition that is consistent with a continental rift setting. Geochemical features of QMB granitoids require a significant heat input to facilitate high-temperature melting of a refractory lower crust. A mafic underplate could provide the necessary heat.

A reconstruction of the QMB tectonic setting is provided in Figure 13. Initial crust formation occurred at 3.1 to 2.8 Ga in the northern Rae domain (Skulski et al., 2003; Schultz et al., 2007; this study). The lower crust of the Rae Domain underwent granitoid extraction at ca. 2.7 and 2.6 Ga creating a LREE- and Th-enriched mid- to upper-crust and leaving a refractory lower crust. West of this established 3.1 to 2.8 Ga crustal precursor zone is evidence for older Mesoarchean to Paleoarchean (3.3 to 3.9 Ga) crust (Fig. 1; Theriault et al., 1994), and east of the 3.1 to 2.8 Ga crustal precursor zone, it has been proposed that ca. 2.7 Ga mafic and ultramafic rocks of the Prince Albert Group were emplaced on a thinned cratonic margin (MacHattie et al., 2007). In consideration of this, MacHattie et al. (2007) proposed that a pre-existing lithospheric architecture played a role in focusing asthenosphere derived melts in the Rae domain during the Archean. This lithospheric architecture may have also helped focus such melts beneath the QMB at ca. 2.5 Ga.

The impingement of asthenosphere-derived mafic magmas beneath the QMB at ca. 2.5 Ga began to melt refractory lower crust and led to emplacement of QMB granitoids in the mid- to upper-crust. Large volumes of mafic magma have not been identified in the QMB and this could be due to several possibilities. Larger volumes of extrusive mafic magmas could have been emplaced in the upper-crust but were removed by erosion to current mid-crustal level. It is also possible that large volumes of mafic magma were not extruded at all and instead mantle melts ponded at the base of the crust. A large volume of ponded mafic magmas within the QMB is crucial to the genesis of this unique, granitoid-dominated terrane. The volume of 2.46 to 2.50 Ga granitoids in the QMB far exceeds that of other similar aged terranes in Laurentia (Krogh, 1996, Ashton et al., 1999; Chamberlain et al., 2003; Rayner et al., 2005) and would have required a vast quantity of heat for mobilization of large volumes of refractory lower crust.

On the basis of the age of the youngest detrital zircon, Schultz et al. (2007) suggested that Sherman basin sedimentation did not begin until ca. 2.44 Ga. This is not supported by the data of the present study. Dating of mafic rocks of inferred volcanic origin within the sedimentary sequence suggests that extension and basin formation began before ca. 2.48 Ga. Granitoid emplacement in the QMB continued until 2.45 Ga, synchronous with extension allowing the Sherman basin to receive primarily 2.45 to 2.50 Ga detritus from exhumed QMB granitoids. Sediment deposition must have ceased before ca. 2.39 Ga when the sediments of the Sherman basin were buried and underwent granulite-grade metamorphism.

7.5 Implication of ca. 2.39 High-grade Metamorphism

There is a distinct time hiatus between the youngest known QMB granitoid (2.46 Ga) and ca. 2.39 Ga granulite metamorphism. On that basis, I propose that formation of the QMB granitoids and granulite metamorphism relate to two separate tectonic events; the former to an incipient continental rift and the latter to orogenesis on the western margin of the Rae Domain. The cause of the ca. 2.3-2.4 Ga orogenesis remains somewhat enigmatic but two possibilities are discussed below: (1) near- and far-field effects of a Slave-Rae

collision at ca. 2.35 Ga, and (2) intraplate orogenesis within an already contiguous Neoarchean continent.

It is widely held that the Talston-Thelon Magmatic Zone (TTMZ; cf. Hoffman, 1987; Chacko et al., 2000; De et al., 2000) represents the suture between the Slave and Churchill provinces, although the timing of collision, and the nature of the TTMz remain controversial. Hoffman (1987) proposed that the Slave and Churchill Provinces were separated by an ocean basin at ~2.0 Ga that closed by subduction beneath the Churchill Province, followed by a Himalayan-style collision at 1.97 Ga. In this model, the TTMz is analogous to the modern-day Himalayas and the QMB to a Tibetan Plateau. If the QMB represented a Tibetan-style orogenic plateau, there should be extensive metamorphic and tectonic reworking of mid-crustal levels at 1.9–2.0 Ga. The data of Schultz et al. (2007) and this study show no evidence of 1.9 to 2.0 Ga magmatism or metamorphism in the eastern and central QMB to within ~150 km of the TTMz boundary. This argues against the QMB being an orogenic plateau at that time. Rather, these findings are consistent with the proposal by Chacko et al. (2000) that the Slave and Churchill Provinces were together in the earliest Paleoproterozoic or Archean. These findings do not preclude the idea that the QMB could represent a 2.39 Ga orogenic plateau.

Evidence for 2.3 to 2.4 Ga orogenesis and proposed eastward-dipping subduction along the western Rae margin exists (Bostock and van Breemen, 1994; Hartlaub et al., 2007) and in particular, ca. 2.35 Ga metamorphism has been identified across strike ~150 km east of the QMB in the Committee Bay Belt (Berman et al., 2005). Collectively these events are now being attributed to the so-called Arrowsmith Orogeny (Berman et al., 2005; Hartlaub et al., 2007). I propose that if 2.3 to 2.4 Ga magmatism was subduction related, it is the result of collision between the Slave and Churchill provinces, at least in the Thelon portion of the TTMz east of the Slave Craton. Indeed the TTMz zone south of the Slave craton has a distinctive history. If the period from 2.3 to 2.4 Ga heralds the arrival of the Slave Province, then evidence of 2.3 to 2.4 Ga arc magmatism within the QMB must all be contained in the ~150 km of rocks east of the TTMz margin not traversed in this study. Alternatively, evidence of 2.3 to 2.4 Ga arc magmatism exists in

the TTMz basement (Frisch and Hunt, 1993; McNicoll et al., 2000,) but is obscured by younger magmatic events. Arc-magmatism and collisional orogeny would have also been unable to contribute detritus to the Sherman Basin, which reflects only 2.45 to 2.50 Ga provenance (Schultz et al., 2007).

The other possibility is that the Slave and Churchill provinces formed a contiguous continent sometime in the late Archean, a proposal which has seen minimal support of early work by Williams et al. (1991), and expanded by Aspler and Chiarenzelli (1998). The work by Aspler and Chiarenzelli (1998) interpreted Paleoproterozoic supracrustal sequences as the products of extension and eventual breakout of a late Archean supercontinent. In contrast, comparisons of igneous rocks from the Slave and Churchill Provinces are rarely made for evidence of assembly and a shared Archean history, despite many similarities. Ca. 2.7 Ga granite-greenstone belts (cf. Slave Province: Isachsen and Bowring, 1997; Churchill Province: Skulski et al., 2003) characterize both these provinces, as does the ubiquitous presence of 2.62 to 2.58 Ga granitoids (cf. Slave Province: Davis and Bleeker, 1999; Churchill Province: Skulski et al., 2003). The implications of such a model are that both phases of TTMz activity (1.9 to 2.0 Ga and 2.3 to 2.4 basement) represent reactivation of an Archean suture. It is then likely that 2.62 to 2.58 Ga granitoid magmatism represents cratonization of this Neoarchean supercontinent. If the QMB was indeed developed within a Neoarchean supercontinent such as Kenorland (cf. Aspler and Chiarenzelli, 1998 and references therein), then an outboard convergent force on the western / southwestern margin of the Slave Province would be required. There is scant evidence on the western Slave margin indicating Paleoproterozoic activity pre-2.3 Ga with the exception of a grouping of detrital grains at ca. 2.3 Ga that occur within the Treasure Lake Group sedimentary rocks of the 1.90 to 1.95 Ga Hottah Terrance (Ghandi and van Breemen, 2005). The Hottah Terrane is believed to contain a 2.0 to 2.4 Ga basement component (Bowring and Podosek, 1989).

8. Conclusions

The Queen Maud Block is not, as originally proposed, a high-grade equivalent of the adjacent Rae Domain. In fact, the segment of the QMB examined in the present study

contains almost no Archean rocks. This study and that of Schultz et al. (2007) shed light on the variety of events that occurred from 2.39 to 2.50 Ga, a period commonly thought to reflect relative tectonomagmatic quiescence within Laurentia. I propose an incipient continental rift in the QMB area and ponding of mantle melts at ca. 2.5 Ga led to mobilization of lower-crust and emplacement of 2.46 to 2.50 Ga granitoids in the mid- and upper crust. The large volume of granitoids emplaced is a unique feature to the QMB in comparison to other 2.46 to 2.50 Ga granitoid occurrences in Laurentia. This indicates an equally large volume of mafic magma ponded at the base of the crust and imparted thermal energy, an inference corroborated by the general lack of mafic rocks within the QMB. The trace-element geochemistry and Sm-Nd isotope signature of 2.46-2.50 Ga QMB granitoids indicates they were extracted from a refractory lower-crust, the result of previous granitoid extractions from the same source region. Extension concurrent with magmatism exposed the 2.46-2.50 Ga granitoids, allowing them to be the primary source of detritus for the Sherman Group metasediments. A tectonic switch eventually terminated extension and basin deposition and the entire area underwent high-grade metamorphism at ca. 2.39 Ga. No evidence of 1.9 to 2.0 Ga metamorphism or magmatism was found within the QMB study area, effectively precluding previous models that propose this is the time of Slave and Churchill suture. The nature of the 2.3 to 2.4 Ga orogeny, although now referred to as the Arrowsmith Orogeny, has not yet been addressed in a detailed tectonic model. I propose that if the 2.3 to 2.4 Ga orogeny is collisional, it is a result of collision between the Slave and Churchill cratons at that time. The QMB would be a hinterland plateau in this collisional event. Another tenable model is that at least the Slave and Churchill provinces represent a contiguous Neoarchean continent and that Paleoproterozoic events in TTMz and QMB are all intracontinental in nature.

In light of the large body of evidence for mafic magmatism, subordinate felsic magmatism and basin initiation at 2.45 to 2.50 Ga elsewhere in Laurentia, specifically the Superior Craton, Wyoming Craton and Hearne Domain (c.f. Heaman, 1997; Aspler and Chiarenzelli, 1998; Heaman, 2004), the QMB provides new evidence that these events also occurred in the northwestern Rae domain. Thus, the presence of 2.46 to 2.50 Ga

magmatism in the QMB suggests it could be placed within a Neoarchean supercontinent consisting of the entirety of the Churchill Province (Rae and Hearne domains), the Superior and Wyoming Cratons and Baltica (cf. Heaman, 1997). Equally likely is the idea that 2.46 to 2.50 Ga magmatism in the QMB should not at all be used as a piercing point in continental reconstructions but simply represents another occurrence of global 2.45 to 2.50 Ga magmatism. It is emphasized here that global-scale magmatic events are not necessarily related to a large point source (i.e. plumes), but may involve multiple discrete mantle melting anomalies.

References

Amelin, Y.V., Heaman, L.M., Semenov, V.S., 1995. U-Pb geochronology of layered mafic intrusions in the eastern Baltic Shield; implications for the timing and duration of Paleoproterozoic continental rifting. Precambrian Research, 75, 31-46.

Ashton, K.E., Heaman, L.M., Lewry, J.F., Hartlaub, R.P., and Shi, R., 1999. Age and origin of the Jan Lake Complex; a glimpse at the buried Archean craton of the Trans-Hudson Orogen. Canadian Journal of Earth Sciences, 36, 185-208.

Aspler, L.B., and Chiarenzelli, J.R., 1998. Two Neoarchean supercontinents? Evidence from the Paleoproterozoic. Sedimentary Geology, 120, 75-104.

Berman, R.G., Sanborn-Barrie, M., Stern, R.A., and Carson, C.J., 2005. Tectonometamorphism at ca. 2.35 and 1.85 Ga in the Rae Domain, western Churchill Province, Nunavut, Canada; insights from structural, metamorphic and in situ geochronological analysis of the southwestern Committee Bay Belt. The Canadian Mineralogist, 43, 409-442.

Bostock, H.H., and van Breemen, O., 1994. Ages of detrital and metamorphic zircons and monazites from a pre-Taltson magmatic zone basin at the western margin of Rae Province. Canadian Journal of Earth Sciences, 31, 1353-1364.

Bowring, S. A. and Podosek F. A, 1989. Nd isotopic evidence from Wopmay Orogen for 2.0-2.4 Ga crust in western North America. Earth and Planetary Science Letters, 94, 217-230.

Chacko, T., De, S.K., Creaser, R.A., and Muehlenbachs, K., 2000. Tectonic setting of the Taltson magmatic zone at 1.9-2.0 Ga: a granitoid-based perspective. Canadian Journal of Earth Sciences, 37, 1597-1609.

Chamberlain, K.R., Frost, C.D., and Frost, B.R., 2003. Early Archean to Mesoproterozoic evolution of the Wyoming Province; Archean origins to modern lithospheric architecture. Canadian Journal of Earth Sciences, 40, 1357-1374.

Creaser, R.A., Erdmer, P., Stevens, R.A. and Grant, S. L., 1997. Tectonic affinity of Nisutlin and Anvil assemblage strata from Teslin tectonic zone, northern Canadian Cordillera: Constraints from neodymium isotope and geochemical evidence. Tectonics, 16, 107-121.

Dahl, P.S., Hamilton, M.A., Wooden, J.L., Foland, K.A., Frei, R., McComba, J.A., and Holm, D.K., 2006. 2480 Ma mafic magmatism in the northern Black Hills, South Dakota; a new link connecting the Wyoming and Superior Cratons. Canadian Journal of Earth Sciences, 43, 1579-1600.

Davis, W. J. and Bleeker, W., 1999. Timing of plutonism, deformation, and metamorphism in the Yellowknife domain, Slave province, Canada. Canadian Journal of Earth Sciences, 36, 1169-1187.

De, S. K., Chacko, T., Creaser, R.A., and Muehlenbachs, K., 2000. Geochemical and Nd-Pb-O isotope systematics of granites from the Taltson magmatic zone, NE Alberta: implications for early Proterozoic tectonics in western Laurentia. Precambrian Research, 102, 221–249.

Fraser, J.A., 1964. Geological notes on northeastern District of Mackenzie, Northwest Territories. Geological Survey of Canada, Paper 63-40, 20 p.

Fraser, J.A., 1978. Metamorphism in the Churchill Province, District of Mackenzie. In: Metamorphism in the Canadian Shield. Geological Survey of Canada, Paper 78-10, 195-202.

Fraser, G., Ellis, D., and Eggins, S., 1997. Zirconium abundance in granulite facies minerals, with implications for zircon geochronology in high-grade rocks. Geology, 25, 607-610.

Frisch, T. and Hunt, P.A., 1993. Reconnaissance U-Pb geochronology of the crystalline core of the Boothia Uplift, District of Franklin, Northwest Territories. In: Radiogenic Age and Isotopic Studies: Report 7; Geological Survey of Canada, Report 93-02, 3-22.

Gandhi, S.S., and van Breemen, O., 2005. SHRIMP U-Pb geochronology of detrital zircons from the Treasure Lake Group; new evidence for Paleoproterozoic collisional tectonics in the southern Hottah Terrane, northwestern Canadian Shield. Canadian Journal of Earth Sciences, 42, 833-845.

Geochemistry of Rocks of the Oceans and Continents (GEOROC) database, used, May 2007. http://georoc.mpch-mainz.gwdg.de/georoc/Entry.html

Geological Survey of Canada, 2006. Canadian Aeromagnetic Data Base. Geoscience Data Repository, Geological Survey of Canada, Earth Sciences Sector, Natural Resources Canada, Government of Canada.

Goldstein, S.L., O'Nions, R.K., and Hamilton, P.J., 1984. A Sm-Nd study of atmospheric dusts and particulates from major river systems. Earth and Planetary Science Letters, 70, 21-236.

Hanmer, S., Sandeman, H.A., Davis, W., Aspler, L.B, Rainbird, R.H., Ryan, J.J., Relf, C., and Peterson, T.D., 2004. Geology and Neoarchean tectonic setting of the central Hearne supracrustal belt, western Churchill Province, Nunavut, Canada. Precambrian Research, 134, 63-83.

Hartlaub, R.P., Chacko, T., Heaman, L.M., Creaser, R.A., Ashton, K.E., and Simonetti, A., 2005. Ancient (Meso- to Paleo-Archean) crust in the Rae Province, Canada; evidence from Sm/Nd and U/Pb constraints. Precambrian Research, 141, 137-153.

Hartlaub, R.P., Heaman, L.M., Chacko, T., and Ashton, K.E., 2007. Circa 2.3-Ga magmatism of the Arrowsmith Orogeny, Uranium City region, western Churchill Craton, Canada.
Journal of Geology, 115, 181-195.

Heaman, L.M., 1997. Global mafic magmatism at 2.45 Ga. Remnants of an ancient large igneous province? Geology, 25, 299-302.

Heaman, L.M., Erdmer, P. and Owen, J.V., 2002. U-Pb geochronologic constraints on the crustal evolution of the Long Range Inlier, Newfoundland. Canadian Journal of Earth Sciences, 39, 845-865.

Heaman, L.M., 2004. 2.5-2.4 Ga global magmatism; remnants of supercontinents or products of superplumes? Abstracts with Programs - Geological Society of America, 36, 255.

Heywood, W.W., 1961. Geological Notes, Northern District of Keewatin. Geological Survey of Canada, Paper 61-18, 9 p.

Hoffman, P.F., 1987. Continental transform tectonics: Great Slave Lake shear zone (ca. 1.9 Ga), Northwest Canada. Geology. 15, 785-788.

Hoffman, P.F., 1988. United plates of America, the birth of a craton; early Proterozoic assembly and growth of Laurentia. Annual Review of Earth and Planetary Sciences. 16, 543-603.

Hoskin, P.W.O., and Black, L.P., 2000. Metamorphic zircon formation by solid-state recrystallization of protolith igneous zircon. Journal of Metamorphic Geology, 18, 423-439.

Hoskin, P.W.O., Schaltegger, U., 2003. The composition of zircon and igneous and metamorphic petrogenesis. Reviews in Mineralogy and Geochemistry, 53, 27-62.

Isachsen, C.E., and Bowring, S.A., 1997. The Bell Lake Group and Anton Complex; a basement-cover sequence beneath the Archean Yellowknife greenstone belt revealed and implicated in greenstone belt formation. Canadian Journal of Earth Sciences, 34, 169-189.

Krogh, T.E., Kamo, S.L., and Bohor, B.F., 1996. Shock metamorphosed with correlated U-Pb discordance and melt rocks with concordant protolith ages indicate an impact origin for the Sudbury structure, In: Hart, S., and Basu, A., (Ed.), Earth Processes: Reading the Isotopic Code. American Geophysical Union, Geophysical Monograph 95, 343–353.

Ludwig, K.R., 2003. Isoplot/Ex, A Geochronological Toolkit for Microsoft Excel, Version 3.0: Berkeley Geochronology Center, Special Publication, 4, 70 p.

MacHattie, T.G., Heaman, L.M., and Creaser, R.A., 2007, The setting and origin of mafic-ultramafic magmatism within the central and northeastern Rae domain. Geological Association of Canada-Mineralogical Association of Canada Annual Meeting, Program with abstracts.

Mahan, K.H., and Williams, M.L., 2005. Reconstruction of a large deep-crustal terrane; implications for the Snowbird tectonic zone and early growth of Laurentia. Geology, 33, 385-388.

McDonough, W.F., and Sun, S.S., 1995. The composition of the Earth. Chemical Geology, 120, 223-253.

McNicoll, V.J., Theriault, R.J., and McDonough, M.R., 2000, Taltson basement gneissic rocks; U-Pb and Nd isotopic constraints on the basement to the Paleoproterozoic Taltson magmatic zone, northeastern Alberta. Canadian Journal of Earth Sciences, 37, 1575-1596

Morris, G.A., Larson, P.B., and Hooper, P.R., 2000. "Subduction style" magmatism in a non-subduction setting; the Colville igneous complex, NE Washington State, USA. Journal of Petrology, 41, 43-67.

Moser, D.E. and Heaman, L.M., 1997. Proterozoic zircon growth in Archean lower crust xenoliths, southern Superior Craton; a consequence of Matachewan Ocean opening. Contributions to Mineralogy and Petrology, 128, 164-175.

Nash, W.P., and Crecraft, H.R., 1985. Partition coefficients for trace elements in silicic magmas. Geochimica et Cosmochimica Acta, 49, 2309-2322.

Pearce, J.A., 1982. Trace element characteristics of lavas from destructive plate boundaries, In: Thorpe R.S. (Ed.), Andesites. John Wiley and Sons, 525-548.

Petrological Database of the Ocean Floor (PetDB) database, used May, 2007. http://www.petdb.org/download_pg.jsp

Peterson, T.D., van Breemen, O., Sandeman, H.A., and Cousens, B., 2002. Proterozoic (1.85-1.75 Ga) igneous suites of the western Churchill Province; granitoid and ultrapotassic magmatism in a reworked Archean hinterland. Precambrian Research, 119, 73-100.

Rayner, N.M., Stern, R.A., and Bickford, M.E., 2005. Tectonic implications of new SHRIMP and TIMS U-Pb geochronology of rocks from the Sask Craton, Peter Lake Domain, and Hearne margin, Trans-Hudson Orogen, Saskatchewan. Canadian Journal of Earth Sciences, 42, 635-657.

Roscoe, S.M., and Card, K.D., 1993. The reappearance of the Huronian in Wyoming; rifting and drifting of ancient continents. Canadian Journal of Earth Sciences, 30, 2475-2480.

Sanborn-Barrie, M., Carr, S.D., and Theriault, R., 2001. Geochronological constraints on metamorphism, magmatism and exhumation of deep-crustal rocks of the Kramanituar Complex, with implications for the Paleoproterozoic evolution of the Archean western Churchill Province, Canada. Contributions to Mineralogy and Petrology, 141, 592-612.

Sandeman, H.A., Hanmer, S., Tella, S., Armitage, A.A., Davis, W.J., and Ryan, J.J., 2006. Petrogenesis of Neoarchaean volcanic rocks of the MacQuoid supracrustal belt; a back-arc setting for the northwestern Hearne Subdomain, western Churchill Province, Canada. Precambrian Research, 144, 140-165.

Schmidberger, S.S., Simonetti, A., Heaman, L.M., Creaser, R.A., and Whiteford, S., 2007. Lu-Hf, in-situ Sr and Pb isotope and trace element systematics for mantle eclogites from the Diavik diamond mine: Evidence for Paleoproterozoic subduction beneath the Slave craton, Canada. Earth and Planetary Science Letters, 254, 55-68.

Schultz, M.E., Chacko, T., Heaman, L.M., Sandeman, H.A., Simonetti, A. and Creaser, R.A., 2007. The Queen Maud Block: A newly recognized Paleoproterozoic (2.4–2.5 Ga) terrane in northwest Laurentia. Geology, 35, 707-710.

Shervais, J.W., 1982. Ti-V plots and the petrogenesis of modern and ophiolitic lavas. Earth and Planetary Science Letters, 59, 101-118.

Simonetti, A., Heaman, L.M., Chacko, T., and Banderjee, N.R., 2006. In situ petrographic thin section U–Pb dating of zircon, monazite, and titanite using laser ablation–MC–ICP-MS. International Journal of Mass Spectrometry, 253, 87–97.

Skulski, T., Sandeman, H.A., MacHattie, T., Sanborn-Barrie, M., Rayner, N., and Byrne, D., 2003. Tectonic setting of 2.73-2.7 Ga Prince Albert Group, Churchill Province, Nunavut. Geological Association of Canada-Mineralogical Association of Canada Annual Meeting, Program with Abstracts.

Stern, R.A., and Amelin, Y., 2003. Assessment of errors in SIMS zircon U-Pb geochronology using a natural zircon standard and NIST SRM 610 glass. Chemical Geology, 197, 111-142.

Stockwell, C.H., 1982. Proposals for time classification and correlation of Precambrian rocks and events in Canada and adjacent areas of the Canadian Shield. Geological Survey of Canada Paper, 80-19, 135.

Streckeisen, A.L., and LeMaitre, R.W., 1979. Chemical approximation to modal QAPF classification of the igneous rocks. Nuess Jahrbuch für Mineralogie, 136, 169-206.

Theriault, R.J., Henderson, J.B. and Roscoe, S.M., 1994. Nd isotopic evidence for early to mid-Archean crust from high grade gneisses in the Queen Maud Block and south of the McDonald Fault, western Churchill Province, Northwest Territories. In: Radiogenic Age and Isotopic Studies: Report 8. Geological Survey of Canada, Current Research 1994-F, 37-42.

Vermeesch, P. 2006. Tectonic discrimination of basalts with classification trees. Geochimica et Cosmochimica Acta, 70, 1839-1848.

Williams, H., Hoffman, P.F., Lewry, J.F., Monger, J.W.H., and Rivers, T., 1991. Anatomy of North America: thematic portrayals of the continent. Tectonophysics, 187, 117-134.

Young M., 2007. Meso- to Neoarchean crustal growth and recycling on northern Baffin Island and correlation of Rae Province rocks across mainland Nunavut and Greenland. Geological Association of Canada-Mineralogical Association of Canada Annual Meeting, Program with abstracts. p. 89

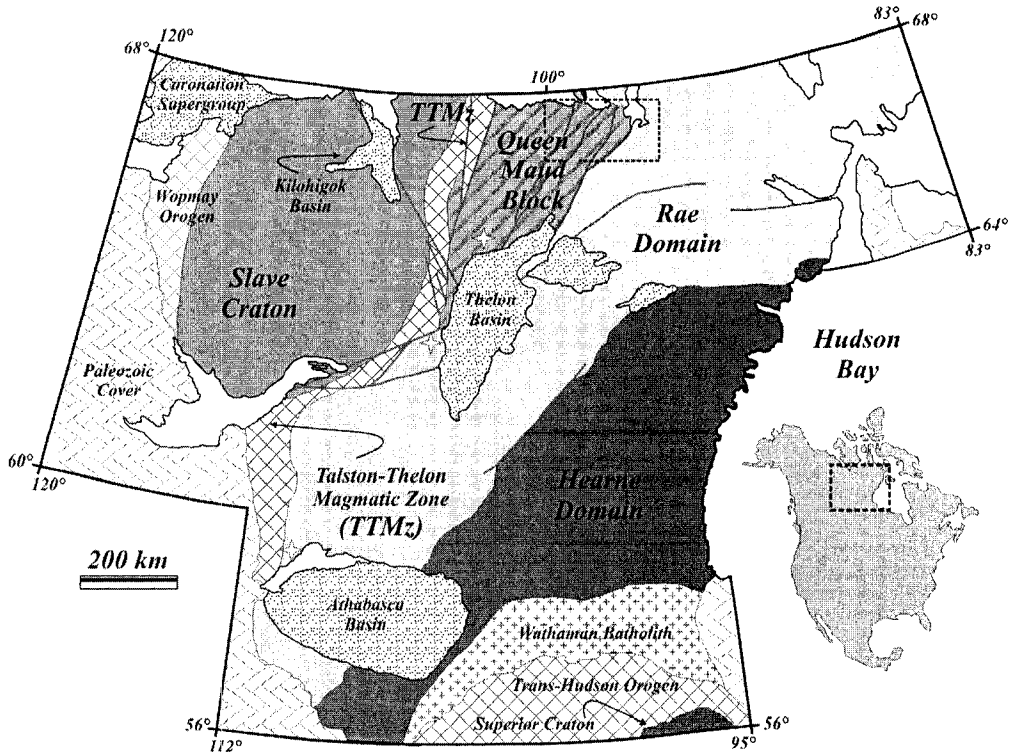

Figure 1. Tectonic elements of northwestern Laurentia including major cratonic blocks, surrounding Paleoproterozoic orogens, and Proterozoic sedimentary basins (modified after Hanmer et al., 2004). The area of the QMB investigated for this study and Schultz et al. (2007) is outlined and detailed in Figure 2. Stars indicate the locations of 3.3 to 3.9 Ga ancient crust (Theriault et al., 1994; Hartlaub et al., 2005).

Figure 2. Spatial compilation of geochronological and Sm-Nd isotope data for the QMB. The broad blue area in the middle represents low magnetic metasediments of the Sherman group, while red, through purple and white areas represent the western and eastern high magnetic areas of the QMB. The white dashed line indicates our proposed eastern boundary for the QMB. Data for this compilation comes from this study and Schultz et al. (2007).

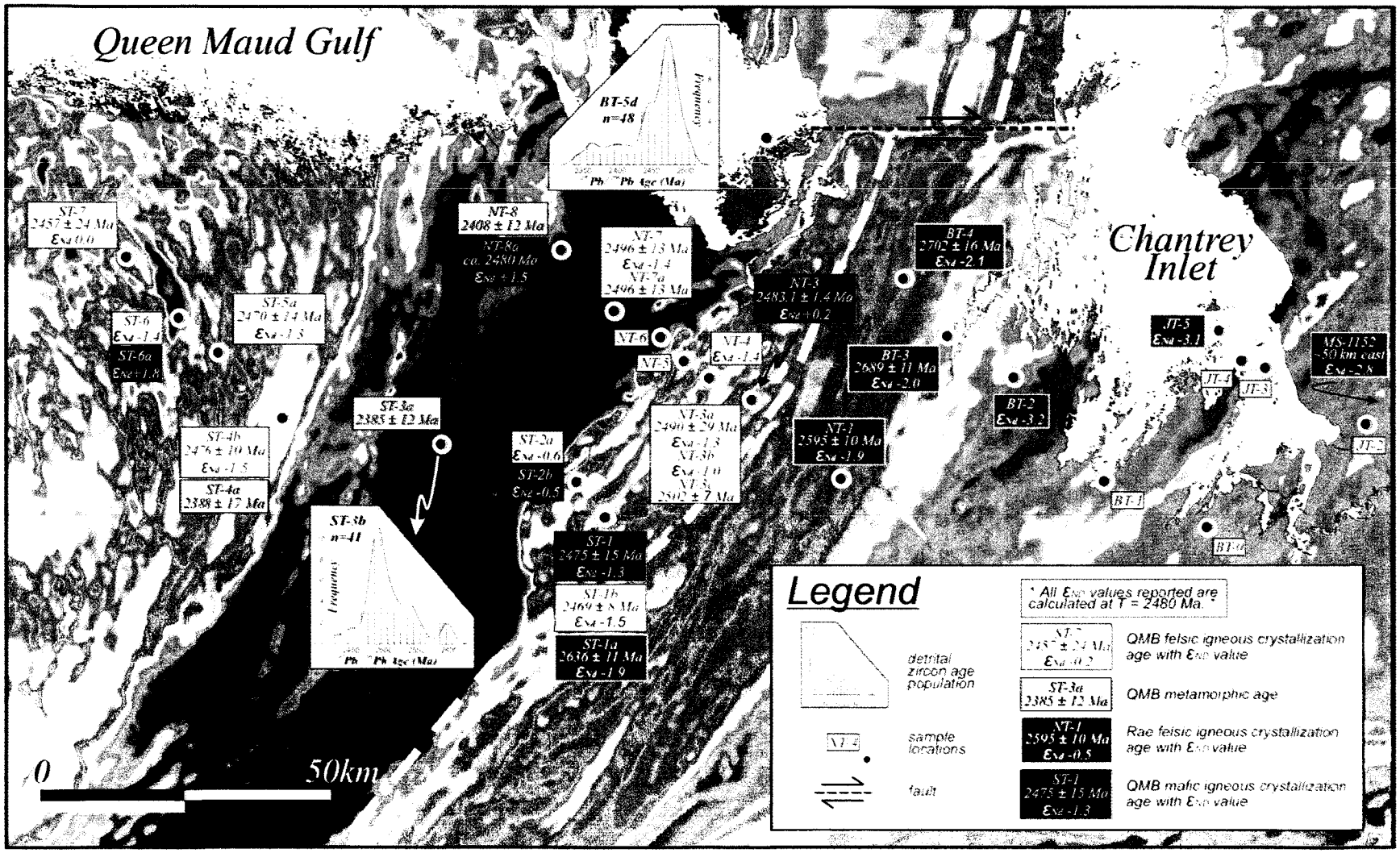

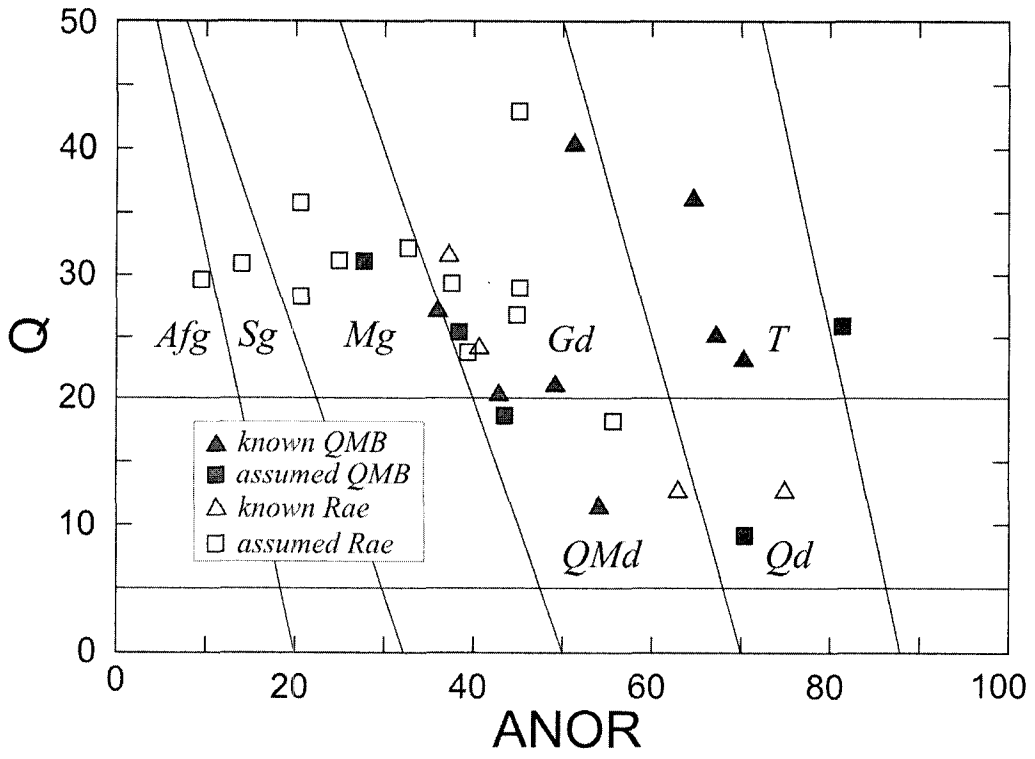

Figure 3. Classification of QMB and Rae domain granitoids using the CIPW normative equivalent to the IUGS classification scheme for granitoids (Streckeisen and LeMaitre, 1979). Parameters: ANOR = normative (An/(Or+An)) x 100, and Q = normative (Q/(Q+Ab+Or+An)) x 100. Fields: Afg, alkali feldspar granite; Sg, syenogranite; Mg, monzogranite; Gd, granodiorite; T, tonalite; QMd, quartz monzodiorite; Qd, quartz diorite.

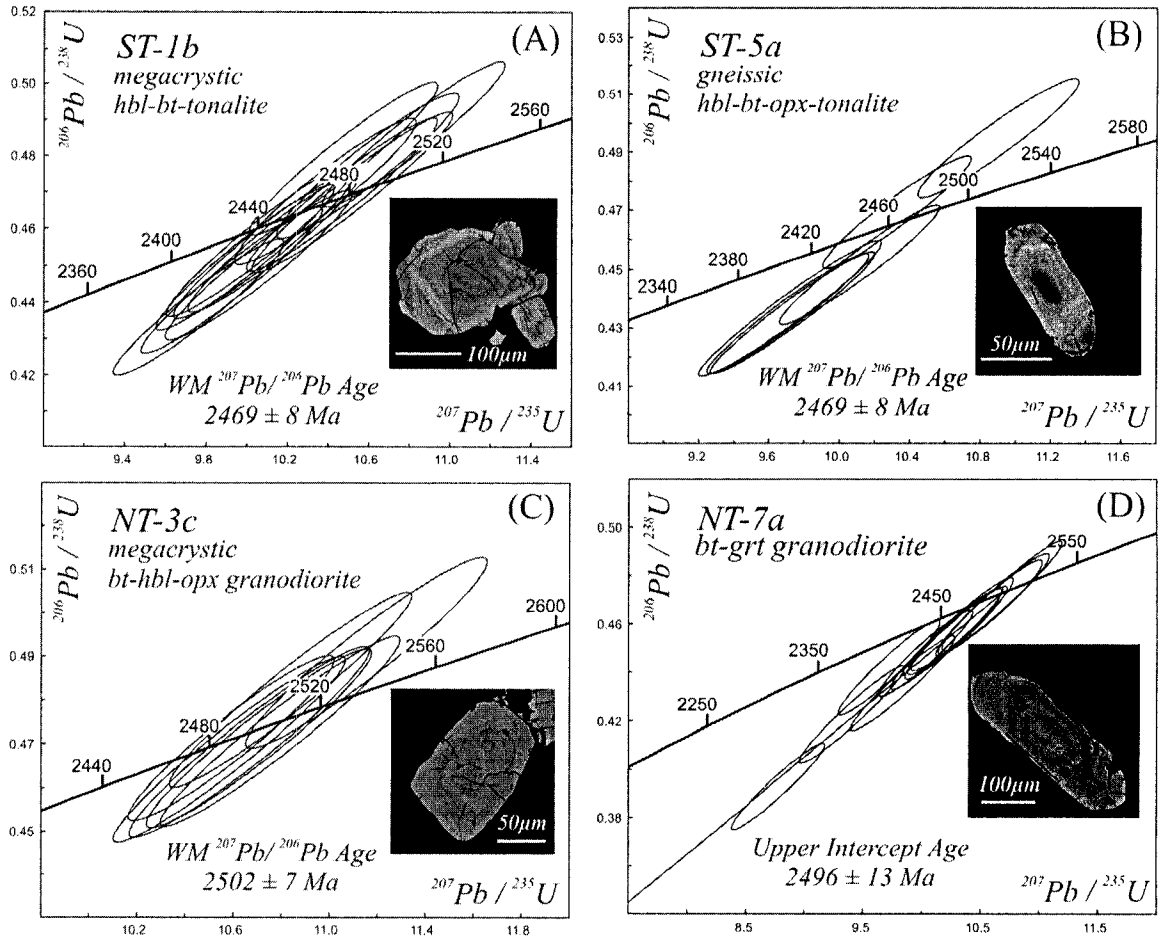

Figure 4. U-Pb results for four granitoid samples from the QMB. Sample locations are indicated in Figure 2. Inset electron backscatter images display examples of oscillatory zoned grains for each sample. Error ellipses are at 2σ levels. All analyses performed using the *in situ* LA-MC-ICP-MS technique.

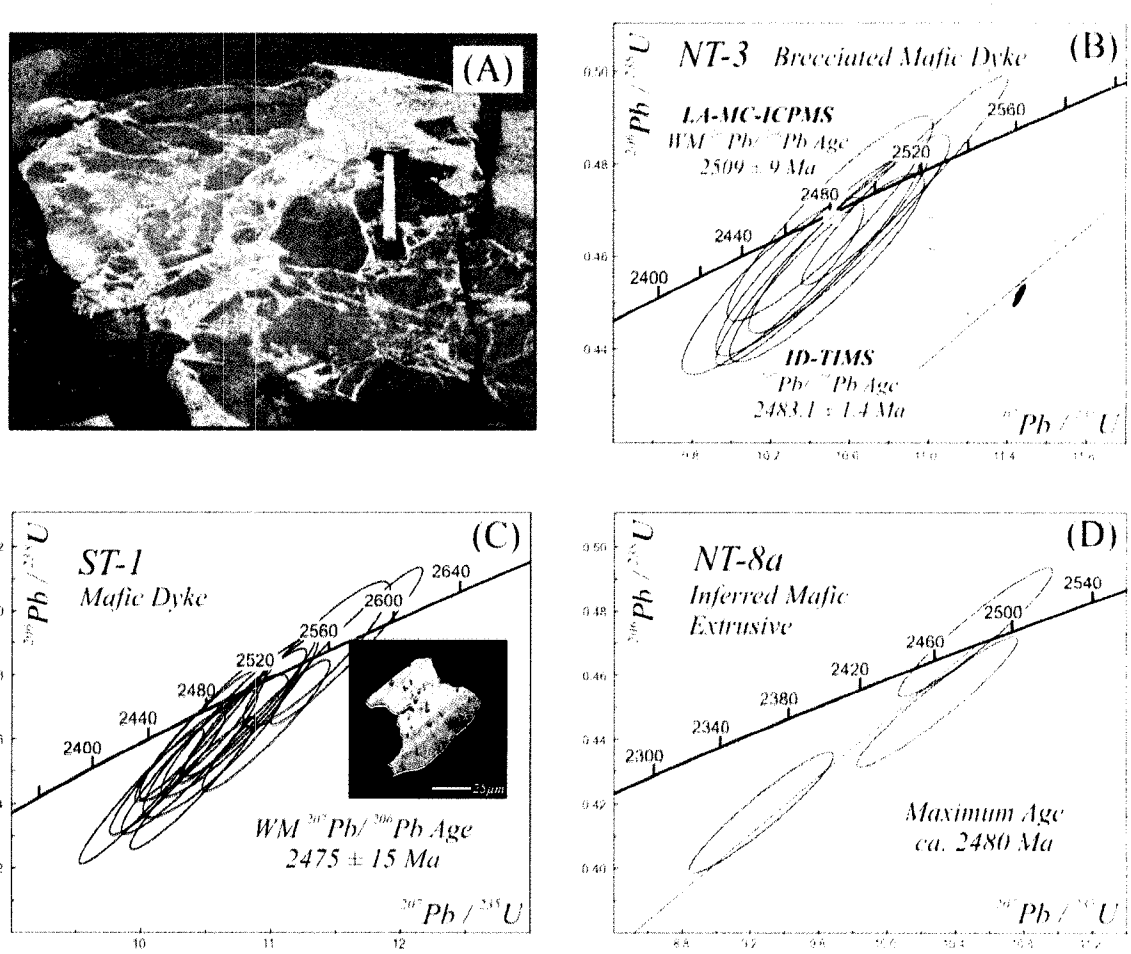

Figure 5. U-Pb results for three mafic samples from the QMB. Sample locations are indicated in Figure 2. The outcrop photo in (a) features the brecciated mafic dyke, NT-3, described in text. The inset in (b) is the ID-TIMS analysis, all other analyses were performed using the *in situ* LA-MC-ICP-MS technique. The inset in (c) is an electron backscatter image of a zircon grain 4 (discussed in text) displaying zoning parallel to the length of the grain

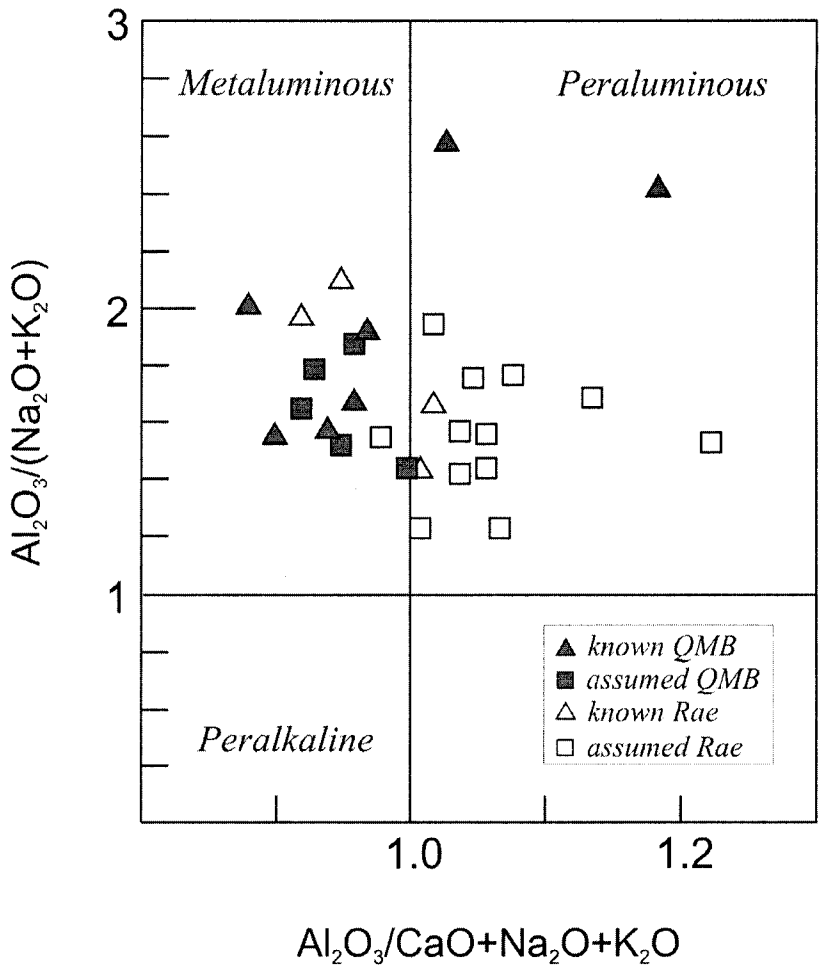

Figure 6. Plot of granitoids from the QMB and Rae domain demonstrating that the bulk of QMB granitoids are metaluminous (A/CNK = molecular $Al_2O_3/CaO + Na_2O + K_2O < 1$), and Rae domain granitoids are largely peraluminous.

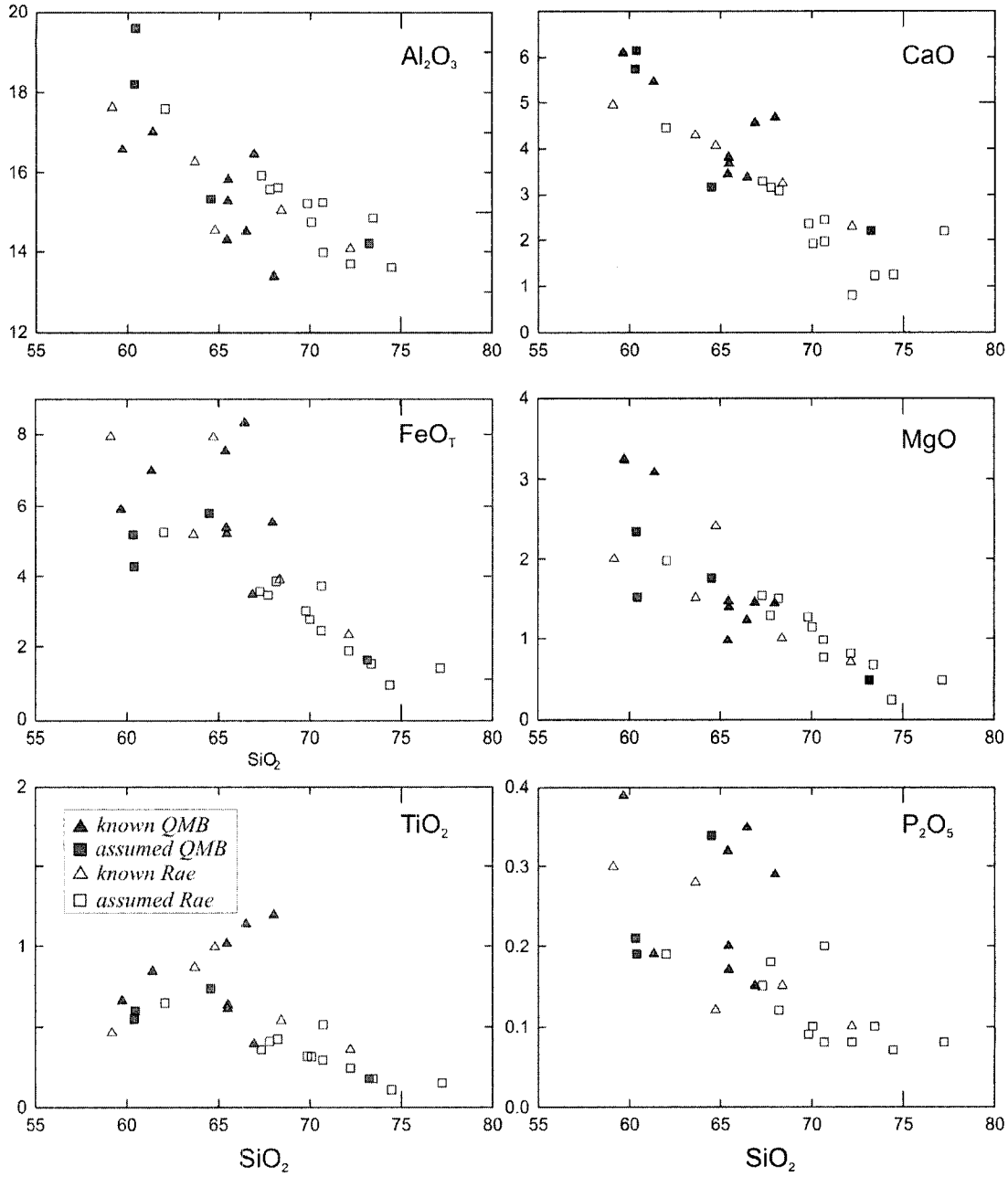

Figure 7. Harker variation diagrams for granitoids and mafic rocks from the QMB and Rae domain. QMB granitoids are generally lower in silica, and are enriched in FeO_T, MgO, TiO_2 and P_2O_5 relative to Rae granitoids. This relative enrichment exhibits greater variability within the QMB granitoids evidenced by the scatter at lower silica. For Al_2O_3 and CaO the QMB and Rae domain granitoids display similar trends.

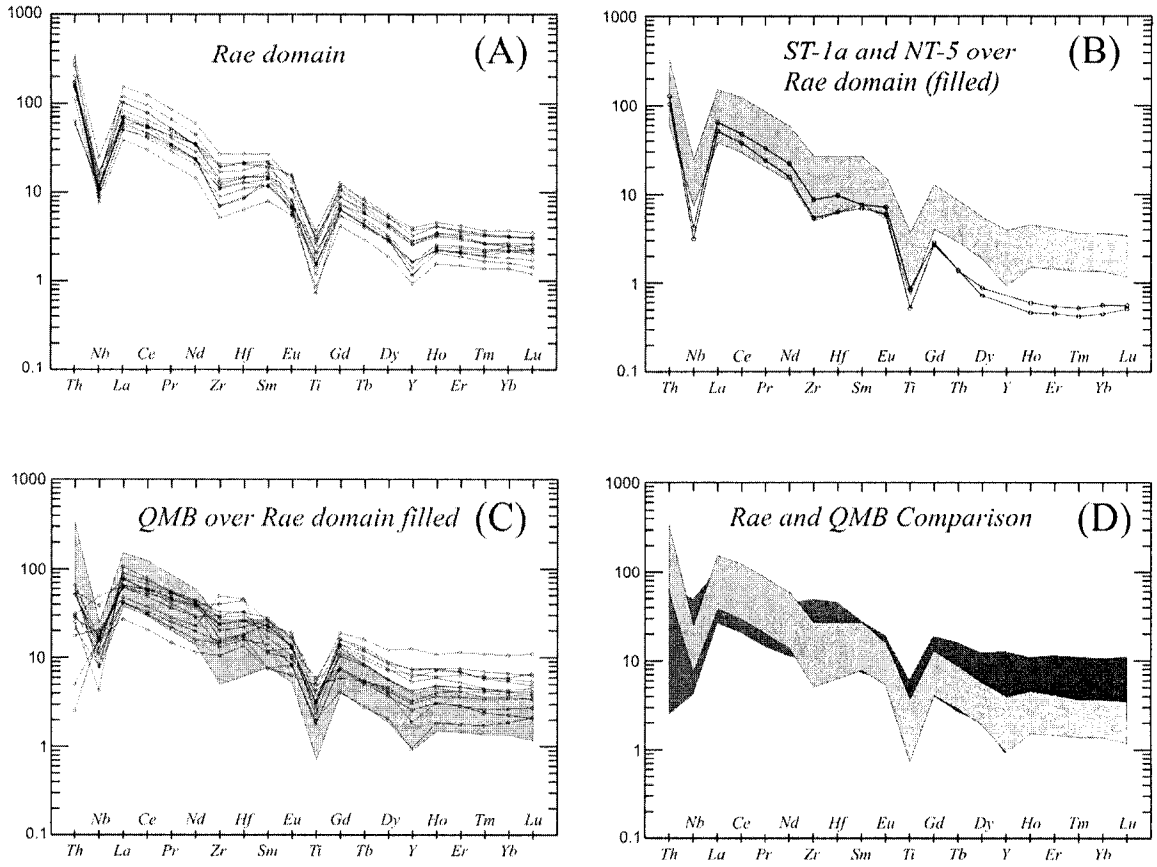

Figure 8. Extended rare earth element plots for granitoids from the QMB and Rae domain (normalization after McDonough and Sun, 1995). (a) Rae domain granitoids. (b) ST-1a and NT-5 over a filled background of (b) highlighting the exaggerated Th/Nb anomaly and greater relative HREE depletion. (c) QMB granitoids plotted over the filled Rae domain range. (d) Comparison of the QMB (dark grey fill) and Rae domain (light grey fill) highlighting Th and LREE depletion and Zr, Hf and HREE enrichment of QMB granitoids relative to Rae granitoids.

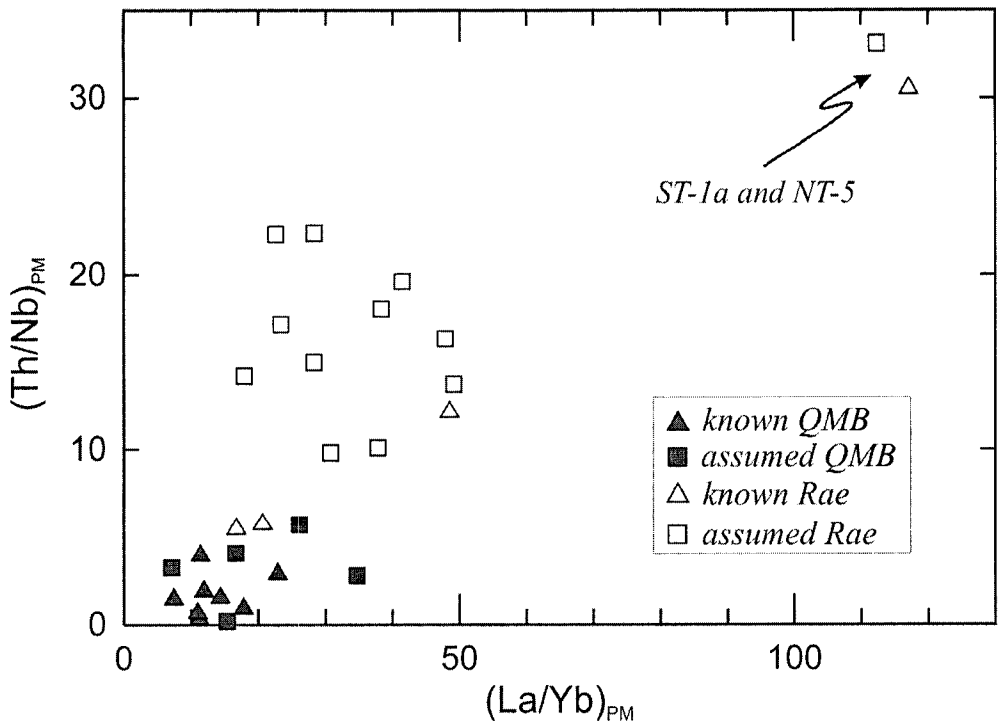

Figure 9. Th/Nb vs. La/Yb plot for granitoids from the QMB and Rae domain (normalization after McDonough and Sun 1995). Plot highlights the low Th/Nb of QMB granitoids and their overall LREE depletion and HREE enrichment relative to Rae domain granitoids. Samples ST-1a and NT-5 form outliers to the Rae domain group and are discussed in text.

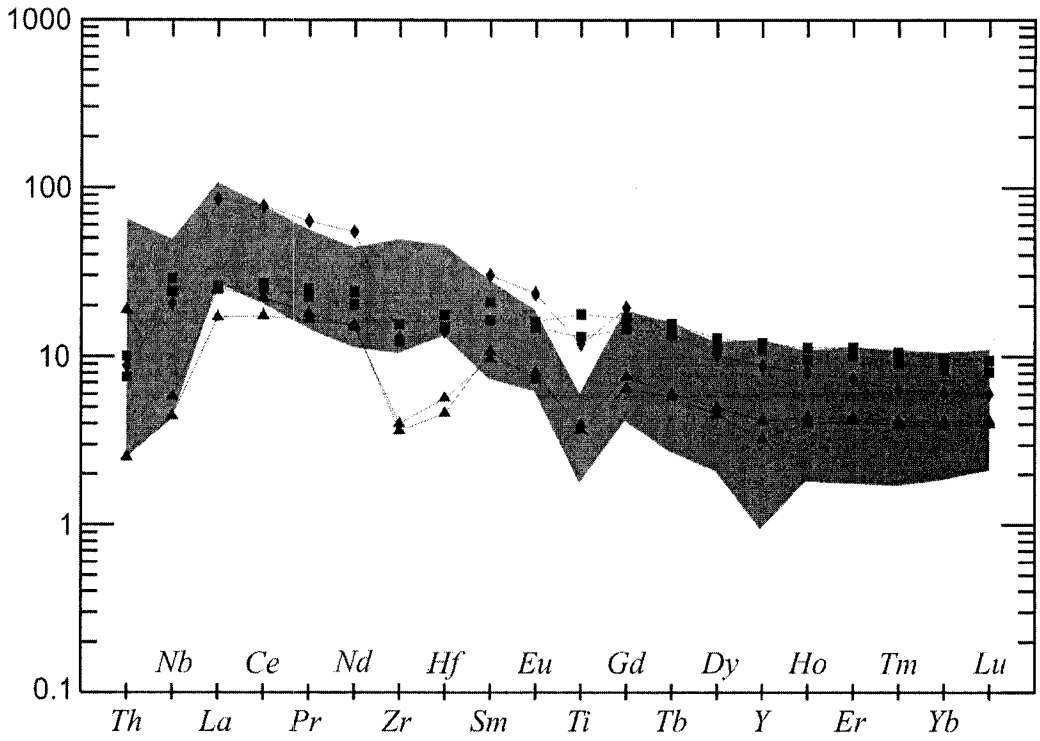

Figure 10. Extended rare earth element plot for mafics rocks from the QMB plotted against the filled range of QMB granitoids. The squares displaying the flat trace element profile are mafic xenolith ST-6a and inferred mafic extrusive NT-8a. Triangles represent mafic dykes ST-2b and NT-3 (higher Th/Nb). The enriched profile in diamonds is mafic dyke ST-1.

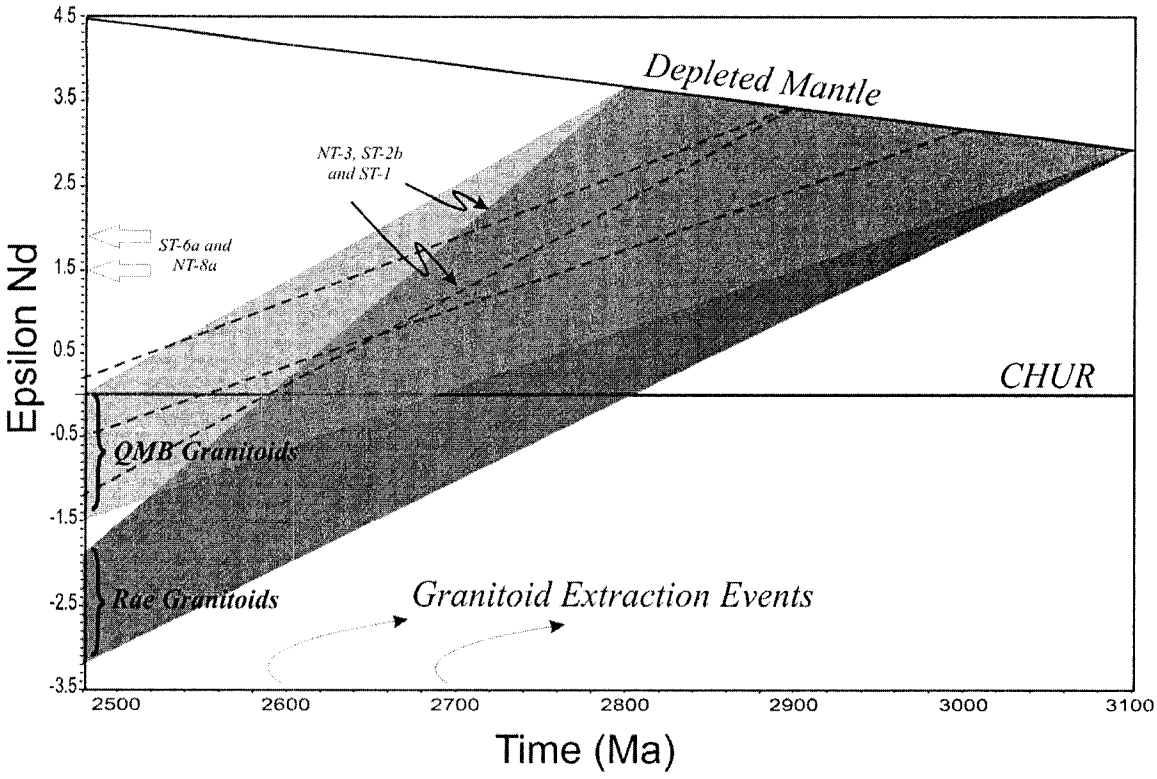

Figure 11. Sm-Nd isotope data for rocks of the QMB and Rae domain. The shaded fields show identical crustal extraction ages for QMB granitoids (light grey fill) and Rae domain (dark grey fill) but a different $^{147}Sm/^{144}Nd$ evolution manifested in the departure of ε_{Nd} values at 2480 Ma. Mafic dykes from the QMB are plotted in dashed lines and ε_{Nd} values at 2480 Ma for mafic xenolith ST-6a and inferred mafic volcanic NT-8a are indicated with arrows. Depleted mantle curve is plotted according to Goldstein et al. (1984).

Figure 12. V vs. Ti comparison plots for basalts from a variety of tectonic environments. The four plots at the top detail basalts from a variety of convergent settings. The bottom four plots include basalts from continental rift settings and the QMB mafic rocks. With the exception of four basalts in the MORB field of the Andean dataset, only basalts from continental rift settings occupy the field with V > 350 ppm and Ti > 14500 ppm. Of the five basalts collected in the QMB, three fall within this field.

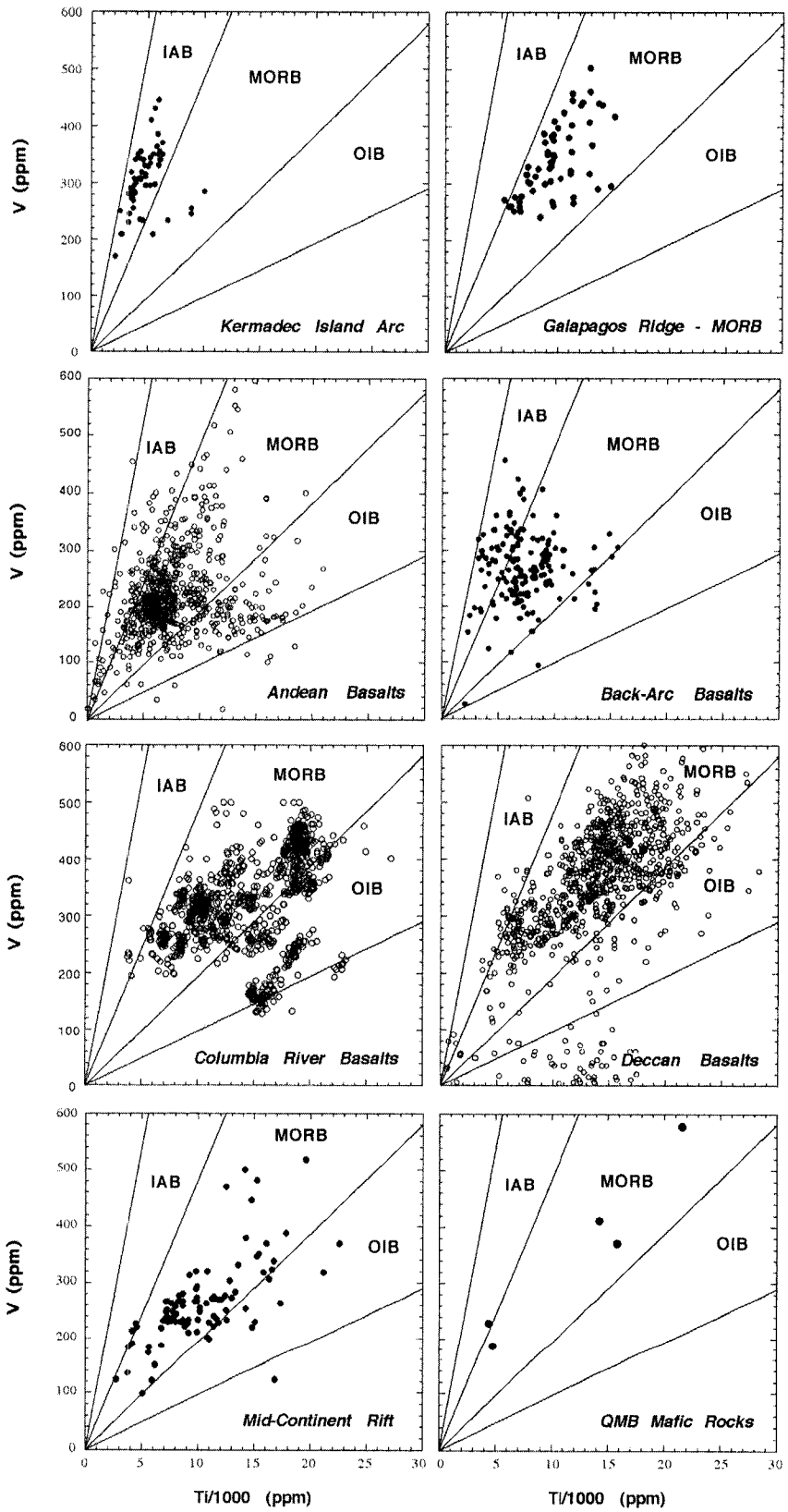

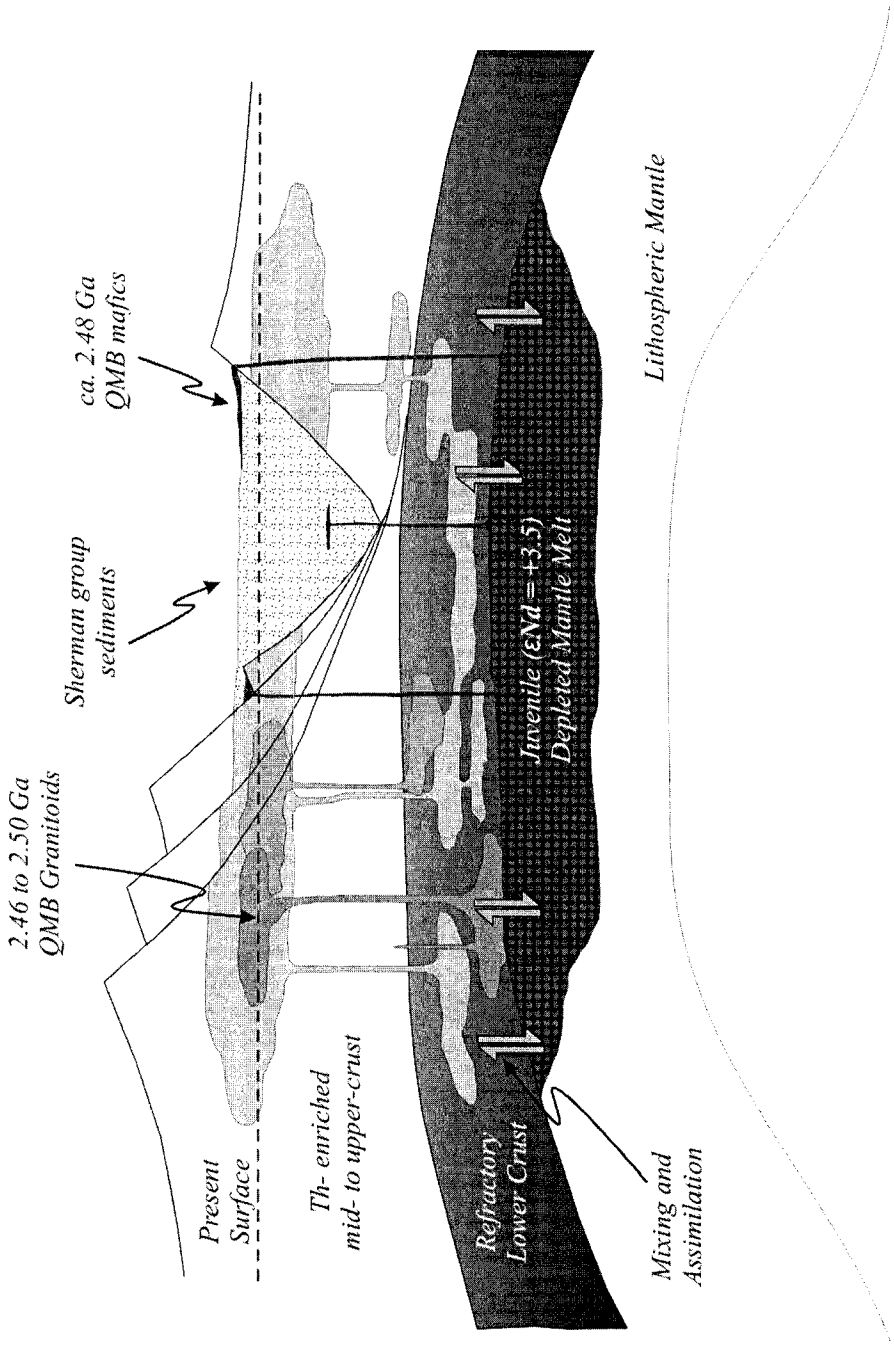

Figure 13. Crustal section of the QMB at ca. 2480 Ga. Mantle melts underplate the QMB, heating and causing mobilization of the refractory lower crust. Mantle melts interact with and are variably contaminated by the lower crust but there is limited direct interaction between juvenile melts and mobilized lower-crustal melts. Coincident extension exhumes newly emplaced granitoids allowing them to be the primary source of detritus to sediments of the Sherman basin. Diagram is not to scale.

Table 1

LA-MC-ICP-MS Geochronology and Sm-Nd isotope summary for rocks collected from the Queen Maud Block and Rae Domain

Sample	Rock Type*		n=[i]	Age (Ma)	MSWD[§]	Age[#] Calculation	Age Interpretation	ε_{Nd} (T_{2480})	T_{DM}[**] (Ga)
Queen Maud Block felsic igneous rocks									
ST-1b	hbl - bt tonalite		13	2469 ± 8	2.3	WM $^{207}Pb/^{206}Pb$	igneous crystallization	-1.5	2.9
ST-2a	opx - hbl - bt quartz monzodiorite							-0.6	2.9
ST-4b[††]	grt - opx - bt tonalite		3	2476 ± 10	0.1	WM $^{207}Pb/^{206}Pb$	igneous crystallization	-1.5	3.0
ST-5a	hbl - bt - opx tonalite		6	2470 ± 14	2.3	WM $^{207}Pb/^{206}Pb$	igneous crystallization	-1.3	2.9
ST-6	bt - hbl - opx tonalite							-1.4	3.0
ST-7[††]	cpx - bt - opx - hbl quartz monzodiorite		3	2457 ± 24	0.6	Model 1	igneous crystallization	0.0	2.8
NT-3a[††]	bt - hbl monzogranite		8	2490 ± 29	3.0	Model 2	igneous crystallization	-1.3	3.1
NT-3b	hbl - bt - opx quartz diorite							-1.0	2.9
NT-3c	bt - hbl - opx ± cpx granodiorite		7	2502 ± 7	0.5	WM $^{207}Pb/^{206}Pb$	igneous crystallization		
NT-4	bt - hbl - granodiorite							-1.4	3.0
NT-7[††]	bt - grt - hbl - opx monzogranite		5	2497 ± 19	3.1	WM $^{207}Pb/^{206}Pb$	igneous crystallization	-1.3	3.0
NT-7a	bt - grt granodiorite		12	2496 ± 13	1.7	Model 2	igneous crystallization		
Queen Maud Block mafic igneous rocks		Th/U							
ST-1	amphibolite	0.736[§§]	13	2475 ± 15	5.3	WM $^{207}Pb/^{206}Pb$	igneous crystallization	-1.3	2.9
ST-2b	mafic granulite							-0.5	3.0
NT-8a	amphibolite	0.241[§§]	3	2479 ± 39	2.7	WM $^{207}Pb/^{206}Pb$	igneous crystallization	1.5	N/A
NT-3	amphibolite		7	2509 ± 9	1.0	WM $^{207}Pb/^{206}Pb$	igneous crystallization	0.2	2.9
NT-3[##]	amphibolite	0.834	1	2483.1 ± 1.4		$^{207}Pb/^{206}Pb$	igneous crystallization	"	"
ST-6a	mafic granulite	0.356[§§]	2	ca. 2420			metamorphic	1.8	N/A
Sherman Group detrital zircon ages									
ST-3[††]	grt - bt pelite		41	2432-2608			age range		
			18	2496 ± 4	0.5	WM $^{207}Pb/^{206}Pb$	primary age node		
BT-5d[††]	opx - bt pelite		48	2345-2513			age range		
			20	2480 ± 4	0.5	WM $^{207}Pb/^{206}Pb$	primary age node		

Table 1
(cont.)
Queen Maud Block U-Pb Monazite Results

Sample	Rock Type*	n = †	Age (Ma)	MSWD§	Age# Calculation	Age Interpretation	ε_{Nd} (T_{2480})	T_{DM}** (Ga)
	grt - crd - sil - Kfs ± bt							
ST-3a††	leucosome	13	2385 ± 5	0.1	WM $^{207}Pb/^{206}Pb$	metamorphic		
		3	2474 ± 10	0.7	WM $^{207}Pb/^{206}Pb$	igneous detrital		
		3	2487 ± 10	0.3	WM $^{207}Pb/^{206}Pb$	igneous detrital		
	grt ± bt							
ST-4a††	leucosome	1	2388 ± 17		$^{207}Pb/^{206}Pb$	metamorphic		
		1	2428 ± 17		$^{207}Pb/^{206}Pb$	igneous detrital		
	bt - grt		2408 ±					
NT-8††	lecosome	2	12	0.4	WM $^{207}Pb/^{206}Pb$	metamorphic		
		1	2515 ± 17		$^{207}Pb/^{206}Pb$	igneous detrital		
Rae Domain felsic igneous rocks								
ST-1a††	musc - bt monzogranite	4	2636 ± 11***	0.8	Model 1	igneous crystallization	-1.9	2.8
NT-1††	tit - bt - hbl - quartz diorite	6	2595 ± 10	0.1	Model 1	igneous crystallization	-1.9	3.0
BT-2	musc - bt granodiorite						-3.2	3.1
BT-3††	hbl - bt - quartz monzodiorite	5	2689 ± 11***	0.8	Model 1	igneous crystallization	-2.0	2.9
BT-4††	bt granodiorite	3	2702 ± 16***	1.2	Model 1	igneous crystallization	-2.1	2.9
JT-5	musc - bt monzogranite						-3.1	3.1
MS-1152	grt - bt - opx granodiorite						-2.8	3.0

* bt = biotite; cpx=clinopyroxene; grt=garnet; hbl=hornblende; opx=orthopyroxene; crd=cordierite; sil=sillimanite; Kfs=potassium feldspar; tit=titanite

† n= # of analyses

§ MSWD = Mean Square Weighted Deviates

WM = weighted mean; Further information can be obtained in Ludwig (2003).

** Calculated using the depleted mantle model of Goldstein et al. 1984

†† Analyses given in Schultz et al. (in press)

§§ Average of values used in age treatment

U-Pb analysis performed by TIMS technique

*** Regressions were anchored at 0 ± 20 Ma. Free regressions could not be calculated or gave negative lower intercepts.

Table 2a
Representative geochemical analyses for felsic igneous rocks of the Queen Maud Block

Sample ID:	ST-2A	ST-5	ST-7	NT-3A	NT-7	*Average*
Domain	QMB	QMB	QMB	QMB	QMB	*QMB*
wt. %						
SiO_2	63.6	66.9	59.7	65.5	65.4	65.1
TiO_2	0.86	0.39	0.66	0.63	1.01	0.74
Al_2O_3	16.3	16.5	16.6	15.8	14.3	15.5
FeO_T	5.18	3.49	5.90	5.21	7.52	5.81
MnO	0.070	0.051	0.132	0.067	0.106	0.09
MgO	1.52	1.46	3.25	1.40	0.98	1.69
CaO	4.30	4.57	6.09	3.69	3.46	4.16
Na_2O	3.54	4.08	3.87	3.85	2.24	3.50
K_2O	3.80	1.77	2.81	3.51	4.55	2.74
P_2O_5	0.28	0.15	0.39	0.17	0.32	0.23
LOI	0.34	0.39	0.63	0.22	0.10	0.29
Mg #	0.37	0.45	0.52	0.35	0.21	0.36
ppm						
Cr	0	45	31	0	0	12
Ni	0	29	12	0	0	10
Co	40	57	41	46	53	50
Sc	17	9	18	16	23	16
V	65	50	111	61	35	67
Cu	0	21	15	0	47	13
Pb	19	24	14	8	17	17
Zn	78	63	81	61	121	89
Rb	63	32	52	83	116	62
Ba	1960	723	1470	1120	1530	1055
Sr	464	552	951	327	195	392
Nb	11.4	7.2	10.4	10.8	25.5	12.3
Hf	8.3	4.8	5.1	7.5	9.1	7.4
Zr	306	159	172	257	317	256
Y	22.2	7.2	24.1	28.9	41.5	20.39
Th	0.25	2.48	0.38	5.16	4.37	2.53
U	0.30	4.12	0.22	1.95	0.71	1.38
La	40.7	27.3	41.6	48.7	50.8	41.8
Ce	87.8	51.5	100.1	100.5	113.2	87.1
Pr	11.3	5.5	13.2	11.7	13.8	10.2
Nd	48.4	19.8	52.9	45.1	55.4	39.6
Sm	9.3	3.1	9.5	9.1	11.4	7.4
Eu	2.93	1.25	2.01	2.05	2.57	1.92
Gd	7.7	2.3	7.3	7.6	10.2	6.1
Tb	1.02	0.27	0.94	1.16	1.59	0.86
Dy	5.1	1.4	4.8	5.8	8.2	4.3
Ho	0.88	0.27	0.91	1.11	1.61	0.80
Er	2.30	0.77	2.78	3.28	4.98	2.32
Tm	0.30	0.11	0.42	0.47	0.74	0.33
Yb	1.80	0.81	2.52	2.91	4.65	2.06
Lu	0.26	0.14	0.36	0.42	0.74	0.31
Th_{PM}/Nb_{PM}	0.2	2.9	0.3	3.9	1.4	2.3
La_{PM}/Yb_{PM}	15	23	11	11	7	16

Table 2b
Representative geochemical analyses for felsic igneous rocks of the Rae Domain

Sample ID:	NT-1	BT-1	BT-4	JT-4	MS04-1152	*Average*
Domain	Rae	Rae	Rae	Rae	Rae	*Rae*
wt. %						
SiO_2	60.4	73.4	64.5	67.7	67.3	68.2
TiO_2	0.60	0.17	0.73	0.41	0.35	0.41
Al_2O_3	19.6	14.9	15.3	15.6	15.9	15.6
FeO_T	4.28	1.52	5.80	3.47	3.58	3.44
MnO	0.057	0.017	0.065	0.061	0.047	0.05
MgO	1.53	0.68	1.77	1.30	1.55	1.30
CaO	6.15	1.25	3.18	3.17	3.31	3.01
Na_2O	4.65	3.55	3.42	3.66	3.42	3.48
K_2O	1.58	3.64	3.36	3.80	3.22	3.51
P_2O_5	0.19	0.10	0.34	0.18	0.15	0.15
LOI	1.04	0.78	0.81	0.40	0.55	0.65
Mg #	0.41	0.47	0.38	0.43	0.46	99.74
ppm						
Cr	0	0	0	0	50	5
Ni	0	0	0	0	0	2
Co	39	54	37	46	51	49
Sc	10	4	10	8	13	8
V	57	18	74	44	40	45
Cu	0	0	19	0	0	2
Pb	18	24	11	22	38	22
Zn	68	32	80	51	49	51
Rb	54	131	121	111	97	116
Ba	973	638	1180	1680	854	902
Sr	871	247	427	559	331	413
Nb	7.1	5.0	8.5	6.9	7.9	8.2
Hf	6.0	1.8	7.6	4.2	4.1	4.3
Zr	223	53	291	150	122	146
Y	15.9	6.6	17.5	9.5	13.4	12.24
Th	4.95	9.03	12.43	13.60	21.34	14.05
U	1.93	1.98	1.37	2.72	1.93	2.90
La	43.8	25.3	99.7	67.1	47.2	50.4
Ce	92.1	50.1	206.1	130.3	96.6	103.3
Pr	11.0	5.1	21.8	13.1	10.2	11.1
Nd	43.9	17.9	74.2	42.9	35.5	38.7
Sm	7.8	3.2	11.0	6.2	6.7	6.6
Eu	2.39	0.84	1.98	1.61	1.25	1.38
Gd	6.0	2.3	6.9	3.5	4.8	4.4
Tb	0.72	0.29	0.79	0.42	0.63	0.55
Dy	3.5	1.3	3.5	1.9	2.9	2.5
Ho	0.61	0.23	0.61	0.33	0.52	0.44
Er	1.65	0.65	1.58	0.90	1.41	1.21
Tm	0.23	0.09	0.22	0.13	0.18	0.17
Yb	1.44	0.61	1.40	0.95	1.13	1.09
Lu	0.21	0.08	0.20	0.15	0.15	0.16
Th_{PM}/Nb_{PM}	5.8	15.0	12.1	16.2	22.4	14.4
La_{PM}/Yb_{PM}	21	28	49	48	28	32

Table 2c
Representative geochemical analyses for mafic igneous rocks of the Queen Maud Block

Sample ID:	ST-1	ST-2B	ST-6A	NT-3	NT-8A
Domain	QMB	QMB	QMB	QMB	QMB
wt. %					
SiO_2	46.1	49.7	48.9	49.7	47.3
TiO_2	2.38	0.80	2.64	0.74	3.60
Al_2O_3	14.7	10.6	12.1	15.2	13.4
FeO_T	15.25	16.22	17.02	9.87	16.97
MnO	0.184	0.272	0.272	0.159	0.309
MgO	5.56	12.90	4.16	8.11	6.08
CaO	9.36	7.79	8.94	10.54	9.52
Na_2O	2.69	1.41	3.29	2.98	0.51
K_2O	0.89	0.20	0.49	0.97	1.37
P_2O_5	1.48	0.18	0.20	0.14	0.37
LOI	1.03	-0.05	-0.30	1.51	0.58
Mg #	0.42	0.61	0.33	0.62	0.42
ppm					
Cr	43	385	0	424	80
Ni	50	148	0	83	50
Co	74	65	40	56	70
Sc	34	46	36	35	46
V	411	186	371	229	578
Cu	51	16	15	33	29
Pb	8	0	0	0	0
Zn	127	134	52	86	157
Rb	20	3	3	16	20
Ba	450	159	186	275	87
Sr	549	325	160	295	276
Nb	13.5	2.9	16.0	3.8	19.0
Hf	4.0	1.3	4.2	1.6	5.0
Zr	143	37	126	51	166
Y	30.1	15.4	35.7	15.5	42.0
Th	0.71	0.18	0.80	1.53	0.61
U	0.43	0.04	0.39	0.41	0.41
La	55.6	11.1	16.8	16.3	16.2
Ce	130.3	29.2	42.2	37.3	45.0
Pr	16.1	4.2	5.8	4.6	6.4
Nd	68.2	19.2	25.6	18.6	30.2
Sm	12.2	4.4	6.7	3.9	8.6
Eu	3.62	1.13	2.30	1.24	2.49
Gd	10.6	4.1	8.0	3.5	9.2
Tb	1.35	0.60	1.34	0.57	1.56
Dy	6.8	3.4	7.6	3.1	8.7
Ho	1.20	0.65	1.43	0.60	1.68
Er	3.24	1.91	4.42	1.84	4.98
Tm	0.44	0.28	0.63	0.27	0.72
Yb	2.69	1.82	3.72	1.72	4.32
Lu	0.41	0.28	0.55	0.27	0.64
Th_{PM}/Nb_{PM}	0.4	0.5	0.4	3.3	0.3
La_{PM}/Yb_{PM}	14	4	3	6	3

Table 3
Sm - Nd isotope analyses for rocks collected from the Queen Maud Block and Rae Domain

Sample	Rock Type	Sm ppm	Nd ppm	$^{147}Sm / ^{144}Nd$	$^{143}Nd / ^{144}Nd$*	T_{DM} Ga†	$\varepsilon_{Nd(2480)}$§
Queen Maud Block mafic igneous							
ST-1	amphibolite	12.540	70.18	0.1080	0.511122 ± 6	2.9	-1.3
ST-2b	mafic granulite	4.416	19.72	0.1354	0.511609 ± 9	3.0	-0.5
ST-6a	mafic granulite	6.880	26.25	0.1585	0.512107 ± 8	2.9	1.8
NT-3	amphibolite	3.665	18.35	0.1208	0.511404 ± 7	2.9	0.2
NT-8a	amphibolite	7.968	29.98	0.1607	0.512127 ± 6	3.0	1.5
Queen Maud Block felsic igneous							
ST-1b	tonalite	5.432	31.69	0.1036	0.511041 ± 7	2.9	-1.5
ST-2a	quartz monzodiorite	9.490	50.56	0.1135	0.511247 ± 7	2.9	-0.6
ST-4b#	tonalite	4.586	24.75	0.1120	0.511179 ± 6	3.0	-1.5
ST-5a	tonalite	2.930	18.87	0.0939	0.510893 ± 7	2.9	-1.3
ST-6	tonalite	2.980	14.37	0.1254	0.511399 ± 7	3.0	-1.4
ST-7#	quartz monzodiorite	9.297	53.24	0.1056	0.511151 ± 8	2.8	0.0
NT-3a#	monzogranite	7.526	34.64	0.1314	0.511504 ± 8	3.1	-1.3
NT-3b	quartz diorite	7.461	48.04	0.0939	0.510907 ± 7	2.9	-1.0
NT-4	granodiorite	10.334	55.00	0.1136	0.511208 ± 8	3.0	-1.4
NT-7#	monzogranite	11.699	61.13	0.1157	0.511244 ± 4	3.0	-1.4
Rae Domain felsic igneous							
ST-1a	monzogranite	3.176	28.16	0.0682	0.510440 ± 7	2.8	-1.9
NT-1#	quartz diorite	7.632	43.19	0.1068	0.511073 ± 9	3.0	-1.9
BT-2	granodiorite	5.956	33.65	0.1070	0.511006 ± 7	3.1	-3.2
BT-3#	quartz monzodiorite	8.969	57.41	0.0945	0.510862 ± 6	2.9	-2.0
BT-4#	granodiorite	11.211	82.60	0.0821	0.510655 ± 6	2.9	-2.1
JT-5	monzogranite	2.637	14.61	0.1091	0.511049 ± 8	3.1	-3.1
MS-1152	granodiorite	4.591	25.34	0.1095	0.511072 ± 15	3.0	-2.8

* Ratio calculated using a ^{147}Sm decay constant = $6.54 \times 10^{-12} yr^{-1}$, uncertainty is reported as 2 sigma

† T_{DM} values are calculated using the depleted mantle model of Goldstein et al., 1984.

§ All ε_{Nd} values are calculated at 2480 Ma

Data from Schultz et al. (2007)

Appendix 1
in situ LA-MC-ICP-MS and TIMS U-Pb for rocks collected from the Queen Maud Block and Rae Domain

in-situ petrographic thin section (zircon) - felsic igneous rocks											Model Ages (Ma)						
Sample	Analysis	^{204}Pb (cps)	^{206}Pb (cps)	$^{207}Pb/^{235}U$	±2σ	$^{206}Pb/^{238}U$	±2σ	rho	$^{207}Pb/^{206}Pb$	±2σ	$^{207}Pb/^{235}U$	±2σ	$^{206}Pb/^{238}U$	±2σ	$^{207}Pb/^{206}Pb$	±2σ	% Disc
ST-1a*	Gr 1.1	0	1416226	10.4874	0.31	0.42935	0.015	0.963	0.17723	0.00190	2479	27	2305	69	2627	18	14.7
	Gr 2.1	0	1060297	11.1518	0.33	0.45194	0.021	0.640	0.17918	0.00187	2536	28	2406	94	2645	17	10.9
	Gr 3.1	0	753640	12.1203	0.36	0.49661	0.022	0.669	0.17704	0.00184	2614	28	2601	95	2625	17	1.2
	Gr 6.1	0	688472	11.0327	0.33	0.44692	0.018	0.996	0.17929	0.00182	2526	28	2383	79	2646	17	11.9
ST-1b	Gr 2.1	0	110037	9.9255	0.36	0.44591	0.016	0.959	0.16094	0.00169	2428	33	2377	87	2466	18	3.6
	Gr 2.2	0	110870	10.0811	0.36	0.45535	0.016	0.956	0.16070	0.00171	2442	33	2419	86	2463	18	1.8
	Gr 3.1†	69	35477	9.7663	0.54	0.47378	0.021	0.785	0.14787	0.00503	2413	49	2500	110	2321	58	-7.7
	Gr 3.2	0	94915	10.3860	0.37	0.47037	0.016	0.950	0.16031	0.00178	2470	32	2485	87	2459	19	-1.1
	Gr 3.3†	0	25962	9.3079	0.36	0.45190	0.017	0.948	0.14856	0.00183	2369	35	2404	91	2329	21	-3.2
	Gr 7.1	0	121315	10.0579	0.38	0.45005	0.017	0.955	0.16243	0.00180	2440	34	2395	89	2481	19	3.5
	Gr 7.2	0	84926	10.0702	0.38	0.45713	0.017	0.960	0.16024	0.00170	2441	34	2427	91	2458	18	1.3
	Gr 9	0	114849	10.5182	0.40	0.47013	0.018	0.962	0.16344	0.00173	2482	35	2484	95	2492	18	0.3
	Gr 12†	0	218918	10.3431	0.34	0.45379	0.015	0.949	0.16583	0.00174	2466	30	2412	79	2516	18	4.1
	Gr 13	0	258222	9.9921	0.36	0.45217	0.016	0.959	0.16063	0.00165	2434	33	2405	86	2462	17	2.3
	Gr 14	0	420009	10.1285	0.34	0.45608	0.015	0.955	0.16142	0.00164	2447	31	2422	81	2471	17	2.0
	Gr 15.1	0	56758	10.4752	0.38	0.47936	0.017	0.954	0.15838	0.00173	2478	33	2524	91	2438	18	-3.5
	Gr 15.2	0	108716	10.5945	0.37	0.47738	0.016	0.948	0.16144	0.00180	2488	32	2516	86	2471	19	-1.8
	Gr 15.3	0	135450	10.8194	0.37	0.48595	0.016	0.954	0.16189	0.00167	2508	31	2553	87	2475	17	-3.1
	Gr 15.4	0	103290	9.7626	0.34	0.43854	0.015	0.953	0.16177	0.00174	2413	32	2344	82	2474	18	5.3
	Gr 16	0	177372	10.4678	0.38	0.46955	0.017	0.960	0.16286	0.00169	2477	33	2482	91	2486	18	0.2
	Gr 17†	0	196846	10.1161	0.37	0.44355	0.016	0.959	0.16506	0.00173	2445	33	2367	86	2508	18	5.6
ST-4b*	Gr 1.1†	0	1046570	10.4195	0.31	0.46739	0.017	0.877	0.15895	0.00274	2473	27	2474	73	2445	29	-1.4
	Gr 4.1	0	796753	11.2982	0.34	0.50558	0.019	0.984	0.16221	0.00164	2548	28	2640	82	2479	17	-7.8
	Gr 4.2	0	867231	10.9085	0.33	0.48895	0.016	0.950	0.16186	0.00165	2515	28	2568	69	2475	17	-4.5
	Gr 5.1†	0	891851	10.1864	0.31	0.46465	0.015	0.947	0.15915	0.00171	2452	27	2462	65	2447	18	-0.7
	Gr 7.1	0	286902	10.7507	0.32	0.48183	0.020	0.709	0.16180	0.00172	2502	28	2537	88	2475	18	-3.0
ST-5a	Gr 1.1†	0	71764	9.6635	0.39	0.44370	0.018	0.964	0.15819	0.00172	2403	37	2367	95	2436	18	2.8
	Gr 1.2†	0	315233	9.2281	0.34	0.42953	0.016	0.962	0.15526	0.00158	2361	33	2304	85	2405	17	4.2
	Gr 2.2	0	421693	10.3271	0.34	0.46959	0.016	0.953	0.15955	0.00163	2465	30	2482	83	2451	17	-1.3
	G 3	0	236401	9.7060	0.38	0.43495	0.017	0.965	0.16228	0.00167	2407	35	2328	90	2480	17	6.1
	Gr 4.1	0	229854	10.1142	0.37	0.45152	0.017	0.961	0.16243	0.00166	2445	33	2402	88	2481	17	3.2
	Gr 4.2	0	233088	9.7183	0.42	0.43656	0.019	0.968	0.16151	0.00178	2408	39	2335	101	2472	19	5.5
	Gr 4.3†	0	196903	7.6276	0.27	0.39195	0.014	0.956	0.14126	0.00150	2188	32	2132	76	2243	18	4.9
	Gr 4.4	0	254945	9.7328	0.38	0.43518	0.017	0.966	0.16235	0.00165	2410	36	2329	92	2480	17	6.1
	Gr 6	0	79400	10.9002	0.37	0.49487	0.017	0.948	0.15998	0.00175	2515	31	2592	88	2455	19	-5.6

In-situ petrographic thin section (zircon) - felsic igneous rocks
continued

Sample	Analysis	^{204}Pb (cps)	^{206}Pb (cps)	$^{207}Pb/^{235}U$	±2σ	$^{206}Pb/^{238}U$	±2σ	rho	$^{207}Pb/^{206}Pb$	±2σ	Model Ages (Ma) $^{207}Pb/^{235}U$	±2σ	$^{206}Pb/^{238}U$	±2σ	$^{207}Pb/^{206}Pb$	±2σ	% Disc
ST-7*	Gr 14.1	0	655854	8.5315	0.26	0.38544	0.015	0.983	0.16156	0.00166	2289	27	2103	68	2472	17	17.5
	Gr 17.1	0	1352600	9.0403	0.27	0.41046	0.014	0.962	0.15982	0.00161	2342	27	2219	65	2454	17	11.4
	Gr 18.1†	0	2215574	8.5001	0.26	0.39551	0.013	0.950	0.15594	0.00158	2286	27	2150	59	2412	17	12.8
	Gr 19.1†	0	2204104	9.2115	0.28	0.42237	0.013	0.947	0.15811	0.00159	2359	27	2273	60	2436	17	8.0
	Gr 20.1	0	1828725	9.6881	0.29	0.43807	0.014	0.952	0.16061	0.00161	2406	27	2344	64	2462	17	5.8
NT-1*	Gr 2.1	0	228668	10.6378	0.32	0.44220	0.017	0.980	0.17449	0.00183	2492	27	2362	75	2601	18	11.0
	Gr 3.1	0	262435	9.3039	0.28	0.38864	0.017	0.701	0.17364	0.00178	2368	27	2118	77	2593	17	21.5
	Gr 5.1	0	174678	11.1693	0.34	0.46555	0.016	0.957	0.17424	0.00182	2537	28	2466	70	2599	17	6.2
	Gr 8.1	0	231948	12.1932	0.37	0.50902	0.019	0.979	0.17410	0.00181	2619	28	2655	82	2597	17	-2.6
	Gr 8.2	0	290176	11.2756	0.34	0.47126	0.017	0.975	0.17420	0.00179	2546	28	2491	76	2598	17	5.1
	Gr 10.2	0	857412	11.5965	0.35	0.48325	0.016	0.952	0.17403	0.00176	2572	28	2543	69	2597	17	2.6
NT-3a*	Gr 1.1	0	135388	4.4531	0.13	0.19513	0.009	0.646	0.16582	0.00172	1722	25	1150	49	2516	17	59.1
	Gr 1.2	0	994354	8.0592	0.24	0.35386	0.013	0.972	0.16416	0.00166	2237	27	1955	61	2499	17	25.3
	Gr 2.1	0	276567	6.4358	0.19	0.28696	0.011	0.978	0.16273	0.00168	2037	26	1628	54	2484	17	39.0
	Gr 4.1	0	309324	6.8515	0.21	0.30840	0.013	0.698	0.16121	0.00168	2092	26	1734	65	2468	18	33.9
	Gr 5.1	0	240520	6.6651	0.20	0.29805	0.010	0.952	0.16249	0.00168	2068	26	1683	49	2482	17	36.5
	Gr 6.1	0	202307	8.2689	0.25	0.37303	0.014	0.976	0.16154	0.00168	2261	27	2045	65	2472	18	20.2
	Gr 7.1	0	244740	9.3824	0.28	0.41295	0.015	0.963	0.16504	0.00169	2376	27	2230	66	2508	17	13.2
	Gr 9.2	0	517837	8.8735	0.27	0.39388	0.014	0.956	0.16284	0.00171	2325	27	2143	62	2485	18	16.3
NT-3c	Gr 1	0	132488	10.7958	0.41	0.47288	0.018	0.962	0.16502	0.00171	2506	34	2496	94	2508	17	0.5
	Gr 2†	0	260316	9.8060	0.34	0.43261	0.015	0.957	0.16500	0.00169	2417	32	2317	81	2508	17	7.6
	Gr 3.1	0	127314	10.5844	0.39	0.46871	0.017	0.962	0.16427	0.00169	2487	34	2478	92	2500	17	0.9
	Gr 3.2	0	87234	11.1543	0.41	0.49086	0.018	0.954	0.16518	0.00183	2536	34	2574	94	2509	19	-2.6
	Gr 4	0	51643	10.6673	0.41	0.47041	0.018	0.960	0.16472	0.00179	2495	35	2485	94	2505	18	0.8
	Gr 5	0	128801	10.7079	0.38	0.47125	0.017	0.955	0.16448	0.00175	2498	33	2489	88	2502	18	0.5
	Gr 8.2	0	186875	10.5917	0.35	0.47126	0.015	0.949	0.16392	0.00172	2488	30	2489	82	2497	18	0.3
	Gr 8.3	0	186345	10.8389	0.41	0.48240	0.018	0.964	0.16348	0.00166	2509	35	2538	96	2492	17	-1.8
NT-7*	Gr 2.1	0	166874	9.3948	0.28	0.41542	0.015	0.960	0.16425	0.00173	2377	27	2241	66	2500	18	12.3
	Gr 3.2†	0	769340	9.8192	0.30	0.44989	0.025	0.532	0.15829	0.00161	2418	27	2397	112	2437	17	2.1
	Gr 4.1†	0	195726	9.5145	0.29	0.42901	0.018	0.719	0.16101	0.00168	2389	27	2303	80	2466	18	7.9
	Gr 7.1	0	711099	9.6162	0.29	0.42950	0.016	0.971	0.16179	0.00163	2399	27	2305	70	2474	17	8.2
	Gr 7.2	0	691940	10.3070	0.31	0.45722	0.017	0.983	0.16367	0.00168	2463	27	2429	77	2494	17	3.2
	Gr 9.1	0	186835	9.7998	0.29	0.42802	0.015	0.961	0.16507	0.00180	2416	27	2299	69	2508	18	10.0
	Gr 9.2	0	99035	9.6086	0.29	0.42161	0.014	0.950	0.16563	0.00179	2398	27	2270	65	2514	18	11.6

In-situ petrographic thin section (zircon) - felsic igneous rocks
continued

Sample	Analysis	^{204}Pb (cps)	^{206}Pb (cps)	$^{207}Pb/^{235}U$	±2σ	$^{206}Pb/^{238}U$	±2σ	rho	$^{207}Pb/^{206}Pb$	±2σ	Model Ages (Ma) $^{207}Pb/^{235}U$	±2σ	$^{206}Pb/^{238}U$	±2σ	$^{207}Pb/^{206}Pb$	±2σ	% Disc
NT-7a	Gr 1.1†	66	71724	9.3218	0.37	0.44341	0.017	0.912	0.15320	0.00251	2370	36	2366	89	2382	28	0.7
	Gr 1.2†	107	126117	8.4882	0.34	0.43423	0.017	0.926	0.14260	0.00216	2285	36	2325	89	2259	26	-2.9
	Gr 1.3†	119	175901	8.9059	0.33	0.42954	0.015	0.931	0.15048	0.00204	2328	33	2304	83	2351	23	2.0
	Gr 2.1	0	138333	10.2137	0.39	0.45414	0.017	0.963	0.16330	0.00169	2454	35	2414	92	2490	17	3.1
	Gr 3	0	175593	9.7221	0.35	0.44197	0.016	0.958	0.15959	0.00168	2409	33	2359	85	2451	18	3.8
	Gr 4	0	428741	9.4082	0.37	0.42271	0.016	0.965	0.16138	0.00167	2379	35	2273	88	2470	18	8.0
	Gr 5.1	0	167734	10.5994	0.35	0.46763	0.015	0.949	0.16432	0.00173	2489	30	2473	81	2501	18	1.1
	Gr 5.2†	0	149951	11.8737	0.45	0.51005	0.019	0.962	0.16906	0.00177	2594	35	2657	101	2548	18	-4.3
	Gr 7.1	0	242664	8.7777	0.33	0.39295	0.014	0.959	0.16194	0.00172	2315	33	2137	79	2476	18	13.7
	Gr 7.2†	0	224377	9.3640	0.70	0.42919	0.032	0.988	0.15778	0.00180	2374	66	2302	171	2432	19	5.3
	Gr 8	0	151767	10.3435	0.36	0.45993	0.016	0.953	0.16308	0.00172	2466	31	2439	84	2488	18	2.0
	Gr 9.1	0	274226	9.8365	0.36	0.43544	0.016	0.961	0.16397	0.00168	2420	33	2330	86	2497	17	6.7
	Gr 9.2	0	140612	10.6129	0.39	0.46833	0.017	0.956	0.16466	0.00178	2490	33	2476	90	2504	18	1.1
	Gr 9.3	0	283798	10.6571	0.44	0.47045	0.019	0.970	0.16446	0.00167	2494	38	2486	102	2502	17	0.7
	Gr 10.1	0	479366	10.0341	0.33	0.44792	0.015	0.951	0.16263	0.00166	2438	30	2386	78	2483	17	3.9
	Gr 10.2	0	422845	10.2921	0.36	0.45647	0.016	0.956	0.16348	0.00167	2461	32	2424	84	2492	17	2.7
	Gr 10.3	0	279742	10.2803	0.33	0.45689	0.015	0.949	0.16307	0.00167	2460	29	2426	77	2488	17	2.5
BT-3*	Gr 1.1	0	189800	13.0992	0.39	0.51388	0.020	0.994	0.18518	0.00192	2686	28	2675	86	2700	17	1.2
	Gr 2.1	0	301590	13.2411	0.40	0.52506	0.020	0.980	0.18291	0.00188	2697	28	2723	83	2679	17	-1.9
	Gr 3.1	0	192623	12.8617	0.39	0.50374	0.024	0.634	0.18539	0.00192	2669	28	2632	102	2702	17	3.2
	Gr 4.1	0	174891	12.3903	0.37	0.48272	0.021	0.700	0.18656	0.00193	2634	28	2541	89	2712	17	7.7
	Gr 5.1	0	318119	12.4249	0.37	0.49340	0.022	0.675	0.18298	0.00189	2637	28	2587	94	2680	17	4.3
BT-4*	Gr 1.1†	0	581913	12.2207	0.37	0.49323	0.018	0.974	0.17996	0.00182	2621	28	2587	78	2653	17	3.1
	Gr 2.1	0	1978067	13.3840	0.40	0.53544	0.023	0.706	0.18154	0.00183	2707	28	2767	95	2667	17	-4.5
	Gr 3.1	0	933203	12.7115	0.38	0.49420	0.020	0.731	0.18683	0.00188	2658	28	2591	87	2714	17	5.6
	Gr 4.1	0	189224	12.1280	0.36	0.47352	0.019	0.990	0.18551	0.00206	2614	28	2501	82	2703	18	9.1
	Gr 5.1†	0	399043	11.1914	0.34	0.47076	0.017	0.967	0.17288	0.00189	2539	28	2489	76	2586	18	4.6

In-situ petrographic thin section (zircon) - mafic igneous rocks											Model Ages (Ma)							
Sample	Analysis	^{204}Pb (cps)	^{206}Pb (cps)	$^{207}Pb/^{235}U$	±2σ	$^{206}Pb/^{238}U$	±2σ	rho	$^{207}Pb/^{206}Pb$	±2σ	$^{207}Pb/^{235}U$	±2σ	$^{206}Pb/^{238}U$	±2σ	$^{207}Pb/^{206}Pb$	±2σ	% Disc	Th/U
ST-1	Gr 1.1	31	55570	11.3529	0.46	0.48662	0.018	0.900	0.16405	0.00291	2553	37	2556	97	2498	30	-2.3	0.512
	Gr 1.2	30	70486	10.4730	0.40	0.46153	0.017	0.918	0.16048	0.00241	2478	34	2446	88	2461	25	0.6	0.682
	Gr 1.3	0	64645	10.9632	0.40	0.46430	0.017	0.942	0.16538	0.00204	2520	33	2459	88	2511	21	2.1	0.48
	Gr 1.4	0	62595	11.5831	0.48	0.48919	0.020	0.961	0.16619	0.00191	2571	38	2567	105	2520	19	-1.9	0.461
	Gr 2.1	0	74053	10.4701	0.42	0.46366	0.019	0.965	0.15878	0.00170	2477	37	2456	98	2443	18	-0.5	1.003
	Gr 2.2	0	68178	10.0057	0.39	0.44236	0.017	0.960	0.15876	0.00175	2435	35	2361	92	2442	19	3.3	1.062
	Gr 2.3	0	47278	10.4029	0.40	0.44631	0.017	0.953	0.16204	0.00187	2471	35	2379	89	2477	19	4.0	0.825
	Gr 2.4†	31	125484	9.4207	0.35	0.42395	0.016	0.948	0.15548	0.00187	2380	34	2278	84	2407	20	5.3	1.073
	Gr 3.1	82	79577	10.7595	0.49	0.46725	0.020	0.930	0.16284	0.00275	2503	42	2471	108	2485	28	0.6	0.979
	Gr 3.2	28	43648	10.5748	0.46	0.45801	0.018	0.891	0.16029	0.00314	2486	39	2431	96	2459	33	1.1	0.74
	Gr 4.1	45	159547	10.2052	0.36	0.44955	0.016	0.940	0.16160	0.00198	2454	32	2393	84	2473	21	3.2	0.899
	Gr 5.1†	81	72587	10.5528	0.45	0.48484	0.020	0.932	0.15307	0.00235	2485	38	2548	103	2380	26	-7.1	0.487
	Gr 5.2†	58	75068	10.8271	0.43	0.48177	0.018	0.933	0.15827	0.00225	2508	36	2535	97	2437	24	-4.0	0.476
	Gr 6.1	28	89753	10.8012	0.39	0.46834	0.016	0.934	0.16199	0.00207	2506	33	2476	86	2477	22	0.0	0.625
	Gr 6.2	30	75077	10.3755	0.43	0.45295	0.018	0.942	0.16137	0.00225	2469	38	2408	97	2470	23	2.5	0.489
	Gr 7.1	0	130951	10.8174	0.43	0.46924	0.019	0.965	0.16188	0.00169	2508	36	2480	98	2475	18	-0.2	0.812
	Gr 7.2†	40	360180	10.0327	0.38	0.46476	0.018	0.961	0.15709	0.00168	2438	35	2461	94	2425	18	-1.5	0.805
ST-6a	Gr 1.1	28	452862	10.2599	0.44	0.47749	0.021	0.971	0.15565	0.00162	2458	39	2516	108	2409	18	-4.5	0.333
	Gr 2.1	50	758583	10.6006	0.67	0.49102	0.031	0.987	0.15629	0.00161	2489	57	2575	163	2416	18	-6.6	0.378
NT-8a	Gr 1.1	45	224821	10.3415	0.39	0.45753	0.017	0.959	0.16376	0.00177	2466	34	2429	91	2495	18	2.7	0.244
	Gr 2.1	41	242347	9.2637	0.35	0.41724	0.015	0.944	0.16180	0.00200	2364	34	2248	82	2475	21	9.2	0.291
	Gr 4.1	44	351005	10.5154	0.37	0.47348	0.016	0.948	0.16090	0.00181	2481	32	2499	87	2465	19	-1.4	0.187
NT-3	Gr 1.1	60	124019	10.4578	0.44	0.45956	0.019	0.946	0.16533	0.00227	2476	38	2438	100	2511	23	2.9	
	Gr 1.2	54	113409	10.4364	0.42	0.46040	0.018	0.922	0.16539	0.00260	2474	37	2441	94	2512	26	2.8	
	Gr 1.3	41	107395	10.4858	0.40	0.45767	0.017	0.909	0.16585	0.00267	2479	35	2429	88	2516	27	3.5	
	Gr 1.4	46	82023	10.2117	0.38	0.45363	0.016	0.888	0.16353	0.00280	2454	34	2411	83	2493	29	3.3	
	Gr 1.5	44	137735	10.5985	0.42	0.46488	0.018	0.927	0.16624	0.00245	2489	36	2461	93	2520	25	2.3	
	Gr 1.6	74	134848	10.5011	0.43	0.46824	0.018	0.922	0.16286	0.00256	2480	37	2476	96	2486	27	0.4	
	Gr 1.7	32	567780	10.8793	0.43	0.47658	0.019	0.966	0.16581	0.00170	2513	36	2512	98	2516	17	0.1	
	Gr 1.9	24	498266	11.1509	0.37	0.48152	0.016	0.952	0.16820	0.00173	2536	31	2534	84	2540	17	0.2	
ID-TIMS 10 grain fragment composite analysis																		
NT-3				10.5075	0.01	0.46861	0.001	0.940	0.16262	0.00006	2481	1	2477	3	2483	1	0.2	0.834

In-situ petrographic thin section (monazite)											Model Ages (Ma)						
Sample	Analysis	^{204}Pb (cps)	^{206}Pb (cps)	$^{207}Pb/^{235}U$	±2σ	$^{206}Pb/^{238}U$	±2σ	rho	$^{207}Pb/^{206}Pb$	±2σ	$^{207}Pb/^{235}U$	±2σ	$^{206}Pb/^{238}U$	±2σ	$^{207}Pb/^{206}Pb$	±2σ	% Disc
ST-3a*	Gr 1.4	0	1117737	8.9391	0.27	0.42358	0.016	0.977	0.15309	0.00157	2331	27	2279	71	2381	17	5.2
	Gr 1.5	0	2016729	9.3149	0.28	0.43821	0.014	0.954	0.15424	0.00155	2369	27	2345	65	2394	17	2.5
	Gr 1.6	0	1728835	9.2486	0.28	0.43787	0.016	0.967	0.15329	0.00154	2363	27	2343	70	2383	17	2.1
	Gr 1.7	0	1722542	9.2437	0.28	0.43744	0.015	0.963	0.15336	0.00154	2362	27	2341	68	2384	17	2.2
	Gr 1.9	0	1350243	9.4298	0.28	0.44623	0.015	0.953	0.15331	0.00155	2380	27	2380	65	2383	17	0.2
	Gr 2.3	0	1262285	9.1431	0.27	0.43313	0.020	0.652	0.15315	0.00159	2352	27	2322	89	2381	18	3.1
	Gr 2.4	0	1546549	9.2401	0.28	0.43878	0.014	0.947	0.15272	0.00154	2362	27	2347	62	2377	17	1.6
	Gr 3.4	0	1998724	10.0697	0.30	0.45327	0.015	0.953	0.16114	0.00165	2441	27	2412	67	2468	17	2.8
	Gr 3.6	0	1800729	10.3013	0.31	0.45956	0.014	0.945	0.16254	0.00166	2462	27	2440	63	2482	17	2.2
	Gr 3.7	0	2284983	10.2972	0.31	0.46196	0.014	0.942	0.16162	0.00167	2461	27	2450	63	2473	17	1.2
	Gr 3.9	0	1385241	9.2990	0.28	0.44015	0.014	0.945	0.15328	0.00156	2368	27	2353	61	2383	17	1.6
	Gr 3.10	0	1280531	9.4299	0.28	0.44662	0.018	0.737	0.15320	0.00156	2380	27	2382	81	2382	17	0.1
	Gr 4.4	0	1422891	10.2183	0.31	0.45653	0.014	0.946	0.16259	0.00167	2454	27	2426	64	2483	17	2.8
	Gr 4.5	0	1402247	10.3015	0.31	0.45680	0.016	0.958	0.16353	0.00166	2462	27	2427	69	2492	17	3.2
	Gr 4.6	0	1320995	10.0907	0.30	0.44803	0.014	0.948	0.16294	0.00165	2443	27	2388	63	2486	17	4.8
	Gr 4.7	0	1627700	8.9641	0.27	0.42149	0.015	0.959	0.15430	0.00159	2334	27	2269	66	2394	18	6.3
	Gr 6.3	0	1021080	9.0061	0.27	0.42372	0.018	0.690	0.15405	0.00162	2338	27	2279	83	2391	18	5.7
	Gr 6.4	0	976991	9.1535	0.27	0.43132	0.014	0.946	0.15349	0.00156	2353	27	2314	61	2385	17	3.7
	Gr 6.5	0	1025864	9.0447	0.27	0.42772	0.013	0.945	0.15341	0.00157	2342	27	2297	60	2384	17	4.4
ST-4a*	Gr 1.1	128	2748913	9.2789	0.28	0.43534	0.018	0.739	0.15374	0.00155	2366	27	2332	79	2388	17	2.9
	Gr 3.1	40	2235400	8.8866	0.27	0.40736	0.013	0.953	0.15740	0.00158	2326	27	2205	61	2428	17	10.9
NT-8*	Gr 1.1	71	2543900	9.3875	0.28	0.43440	0.014	0.953	0.15589	0.00156	2376	27	2327	64	2412	17	4.2
	Gr 1.2	41	3008192	9.4437	0.28	0.43892	0.014	0.946	0.15520	0.00158	2382	27	2348	61	2404	17	2.9
	Gr 2.1	47	1257906	10.5892	0.32	0.46093	0.015	0.950	0.16572	0.00167	2487	27	2446	65	2515	17	3.4

Detrital Zircon Mounts

Sample	Analysis	^{204}Pb (cps)	^{206}Pb (cps)	$^{207}Pb/^{235}U$	±2σ	$^{206}Pb/^{238}U$	±2σ	rho	$^{207}Pb/^{206}Pb$	±2σ	Model Ages (Ma) $^{207}Pb/^{235}U$	±2σ	$^{206}Pb/^{238}U$	±2σ	$^{207}Pb/^{206}Pb$	±2σ	% Disc
BT-5d*	E5	0	307118	10.4871	0.31	0.47080	0.015	0.946	0.16181	0.00168	2478	27	2489	66	2475	17	-0.6
	E6	0	718154	10.7598	0.32	0.48158	0.016	0.950	0.16231	0.00164	2502	27	2536	67	2480	17	-2.7
	E8	0	337349	10.6633	0.32	0.47832	0.017	0.964	0.16184	0.00167	2494	27	2522	74	2475	17	-2.2
	E10	0	414563	10.8500	0.33	0.48445	0.016	0.955	0.16253	0.00169	2510	28	2549	71	2482	18	-3.1
	E11	0	494694	10.8476	0.33	0.48777	0.017	0.956	0.16157	0.00165	2510	28	2563	71	2472	17	-4.4
	E15	0	302723	10.6466	0.32	0.47746	0.016	0.951	0.16264	0.00168	2492	27	2518	69	2483	17	-1.6
	E16	0	662055	10.3235	0.31	0.47114	0.015	0.944	0.15928	0.00165	2464	27	2491	65	2448	18	-2.0
	E17	0	617769	10.6574	0.32	0.47826	0.016	0.956	0.16186	0.00164	2493	27	2522	70	2475	17	-2.2
	E18	0	500513	10.5601	0.32	0.47324	0.016	0.958	0.16217	0.00165	2485	27	2500	71	2478	17	-0.9
	E20	0	575629	9.8427	0.30	0.45625	0.015	0.951	0.15690	0.00162	2420	27	2425	66	2422	17	0.0
	E21	0	367511	10.3107	0.31	0.45892	0.015	0.953	0.16326	0.00168	2463	27	2437	68	2490	17	2.6
	E22	0	359110	10.1048	0.30	0.45928	0.015	0.948	0.16001	0.00167	2444	27	2438	66	2456	18	0.9
	E23	0	1680984	10.6656	0.32	0.48463	0.016	0.953	0.15978	0.00163	2494	27	2549	69	2453	17	-4.6
	E24	0	449287	10.2248	0.31	0.46484	0.016	0.962	0.16111	0.00163	2455	27	2463	71	2467	17	0.3
	E25	0	922580	10.7032	0.32	0.48041	0.016	0.946	0.16163	0.00173	2497	27	2531	68	2473	18	-2.7
	E26	0	508616	9.9949	0.30	0.45647	0.016	0.968	0.15917	0.00162	2434	27	2426	72	2447	17	1.1
	E27	0	892802	10.5182	0.32	0.47824	0.016	0.956	0.16034	0.00163	2481	27	2522	70	2459	17	-3.0
	E28	0	503769	10.7146	0.32	0.48066	0.017	0.959	0.16249	0.00166	2498	27	2532	72	2482	17	-2.4
	E29	0	708633	9.5011	0.29	0.45501	0.015	0.952	0.15171	0.00154	2387	27	2419	66	2365	17	-2.6
	E30	0	814739	10.6458	0.32	0.47572	0.017	0.963	0.16263	0.00165	2492	27	2511	72	2483	17	-1.2
	F5	0	689327	9.9549	0.30	0.46155	0.018	0.993	0.15661	0.00167	2430	27	2448	81	2419	18	-1.3
	F8	0	1010583	9.8172	0.29	0.45880	0.017	0.967	0.15548	0.00165	2417	27	2436	73	2407	18	-1.4
	F14	0	433237	10.8233	0.32	0.48254	0.016	0.953	0.16291	0.00166	2508	28	2540	69	2486	17	-2.5
	F15	0	414851	10.7936	0.32	0.48168	0.016	0.951	0.16314	0.00173	2505	28	2537	70	2489	18	-2.2
	F16	0	407733	10.3231	0.31	0.47330	0.017	0.961	0.15830	0.00170	2464	27	2500	73	2438	18	-3.0
	F18	0	396694	10.7051	0.32	0.47467	0.016	0.958	0.16317	0.00169	2497	27	2506	71	2489	17	-0.7
	F20	0	710812	10.3115	0.31	0.47093	0.017	0.967	0.15901	0.00162	2463	27	2490	73	2445	17	-2.1
	F23	0	620052	9.4890	0.28	0.45466	0.015	0.945	0.15141	0.00167	2386	27	2418	67	2362	19	-2.7
	G2	0	364706	10.5949	0.32	0.47549	0.015	0.947	0.16185	0.00167	2488	27	2510	66	2475	17	-1.6
	G4	0	375870	9.5254	0.29	0.45007	0.015	0.952	0.15413	0.00165	2390	27	2397	68	2392	18	-0.2
	G10	0	661258	10.4457	0.31	0.47265	0.018	0.984	0.16056	0.00163	2475	27	2497	79	2462	17	-1.6
	G11	0	436769	5.8959	0.18	0.36337	0.012	0.947	0.11785	0.00123	1960	26	2000	55	1924	19	-4.5
	G13	0	421029	9.6957	0.29	0.45442	0.015	0.955	0.15499	0.00162	2406	27	2417	68	2402	18	-0.7
	G15	0	328153	9.1919	0.28	0.43822	0.015	0.961	0.15226	0.00157	2357	27	2345	69	2371	18	1.4
	G20	0	901652	9.3489	0.28	0.45315	0.016	0.957	0.14994	0.00156	2372	27	2411	69	2345	18	-3.3
	G21	0	854513	9.8775	0.30	0.46824	0.016	0.955	0.15334	0.00157	2423	27	2478	69	2384	17	-4.7

Detrital Zircon Mounts
continued

Sample	Analysis	^{204}Pb (cps)	^{206}Pb (cps)	$^{207}Pb/^{235}U$	±2σ	$^{206}Pb/^{238}U$	±2σ	rho	$^{207}Pb/^{206}Pb$	±2σ	Model Ages (Ma) $^{207}Pb/^{235}U$	±2σ	$^{206}Pb/^{238}U$	±2σ	$^{207}Pb/^{206}Pb$	±2σ	% Disc
BT-5d*	G22	0	1007758	10.5983	0.32	0.48350	0.017	0.962	0.15922	0.00161	2488	27	2545	73	2447	17	-4.7
cont	G23	0	1007758	10.5983	0.32	0.48350	0.017	0.962	0.15922	0.00161	2488	27	2545	73	2447	17	-4.7
	G25	0	693925	10.6696	0.32	0.47878	0.016	0.959	0.16194	0.00164	2494	27	2524	71	2476	17	-2.2
	G26	0	772828	7.6394	0.23	0.41111	0.015	0.969	0.13485	0.00138	2189	27	2222	68	2162	18	-3.2
	G28	0	821799	10.8604	0.33	0.49010	0.017	0.964	0.16157	0.00163	2511	28	2573	74	2472	17	-4.9
	Gr 8	0	910163	11.1815	0.34	0.49459	0.017	0.959	0.16486	0.00170	2538	28	2593	73	2506	17	-4.1
	Gr 16	0	927897	11.0255	0.33	0.48795	0.018	0.972	0.16431	0.00166	2525	28	2564	76	2500	17	-3.0
	Gr 18	0	410769	10.5911	0.32	0.46595	0.015	0.951	0.16469	0.00168	2488	27	2468	67	2504	17	1.9
	Gr 20	0	662488	10.5039	0.32	0.46751	0.017	0.966	0.16322	0.00168	2480	27	2475	73	2489	17	0.8
	Gr 21	0	404481	10.1863	0.31	0.45492	0.017	0.985	0.16265	0.00168	2451	27	2419	77	2483	17	3.2
	Gr 25	0	1258219	11.0034	0.33	0.48808	0.018	0.977	0.16396	0.00167	2523	28	2564	78	2497	17	-3.2
	Gr 26	0	630597	11.3718	0.34	0.49957	0.016	0.947	0.16556	0.00171	2554	28	2614	69	2513	17	-4.8
ST-3*	C2	0	209906	11.9522	0.36	0.49896	0.016	0.945	0.17413	0.00180	2600	28	2611	67	2598	17	-0.5
	C3	0	268256	10.8880	0.33	0.48351	0.015	0.943	0.16319	0.00173	2513	28	2545	66	2489	18	-2.6
	C6	0	76928	10.2332	0.31	0.46041	0.015	0.864	0.16222	0.00273	2456	27	2443	67	2479	28	1.8
	C9	0	77320	9.7321	0.29	0.44439	0.016	0.953	0.16018	0.00191	2409	27	2372	72	2458	20	4.2
	C12	0	155731	10.2172	0.31	0.45871	0.016	0.963	0.16215	0.00171	2454	27	2436	72	2478	18	2.1
	C16	0	96788	11.3701	0.34	0.48693	0.019	0.980	0.16964	0.00183	2554	28	2559	81	2554	18	-0.2
	C17	0	166021	10.7110	0.32	0.47510	0.015	0.942	0.16413	0.00173	2498	27	2508	65	2499	18	-0.3
	C18	0	191182	10.8831	0.33	0.48211	0.016	0.955	0.16381	0.00169	2513	28	2539	71	2495	17	-2.0
	C25	0	700041	11.1547	0.33	0.49403	0.016	0.948	0.16352	0.00171	2536	28	2590	70	2492	18	-4.7
	C26	0	289028	11.7701	0.35	0.50395	0.016	0.939	0.16910	0.00181	2586	28	2633	67	2549	18	-3.9
	C27	0	300900	11.1603	0.33	0.49321	0.017	0.937	0.16449	0.00200	2536	28	2587	73	2502	20	-4.0
	C30	0	120294	10.4626	0.31	0.45734	0.016	0.963	0.16585	0.00174	2476	27	2430	72	2516	18	4.2
	B2	0	125384	26.8543	0.81	0.67743	0.023	0.957	0.28764	0.00301	3378	29	3337	89	3405	16	2.6
	B3	0	123460	11.3255	0.34	0.48075	0.016	0.956	0.17090	0.00178	2550	28	2533	71	2566	17	1.7
	B5	0	276251	11.5607	0.35	0.49735	0.017	0.962	0.16843	0.00171	2569	28	2604	74	2542	17	-2.9
	B6core	0	970318	11.7395	0.35	0.50603	0.016	0.948	0.16827	0.00170	2583	28	2642	69	2541	17	-4.8
	B7	0	184324	11.2057	0.34	0.47934	0.020	0.726	0.16941	0.00177	2540	28	2526	86	2552	17	1.3
	D1	0	239276	10.9917	0.33	0.48658	0.016	0.940	0.16398	0.00180	2522	28	2558	67	2497	18	-2.8
	D2	0	479483	10.8287	0.32	0.48193	0.015	0.936	0.16262	0.00184	2508	28	2538	67	2483	19	-2.6
	D4	0	198411	10.6855	0.32	0.46842	0.016	0.956	0.16504	0.00172	2496	27	2479	70	2508	17	1.5
	D5	0	480659	10.4481	0.31	0.47610	0.015	0.943	0.15963	0.00166	2475	27	2512	65	2452	18	-2.9

Detrital zircon mounts
continued

Sample	Analysis	^{204}Pb (cps)	^{206}Pb (cps)	$^{207}Pb/^{235}U$	±2σ	$^{206}Pb/^{238}U$	±2σ	rho	$^{207}Pb/^{206}Pb$	±2σ	Model Ages (Ma) $^{207}Pb/^{235}U$	±2σ	$^{206}Pb/^{238}U$	±2σ	$^{207}Pb/^{206}Pb$	±2σ	% Disc
ST-3*	A5	0	208158	11.1142	0.33	0.48385	0.015	0.941	0.16690	0.00175	2532	28	2546	64	2527	18	-0.8
cont	A6	0	54298	10.6368	0.32	0.46418	0.016	0.939	0.16639	0.00207	2492	27	2460	71	2522	21	3.0
	A7	0	231611	11.1739	0.34	0.48272	0.016	0.956	0.16797	0.00171	2537	28	2541	70	2538	17	-0.1
	A8	0	178809	10.6003	0.32	0.46937	0.016	0.956	0.16394	0.00175	2488	27	2483	71	2497	18	0.8
	A11	0	307847	10.0945	0.30	0.46681	0.017	0.966	0.15777	0.00164	2443	27	2472	73	2432	18	-1.9
	A12	0	271305	11.0019	0.33	0.49085	0.016	0.944	0.16300	0.00179	2523	28	2576	70	2487	18	-4.3
	A14	0	292317	10.8789	0.33	0.48252	0.015	0.945	0.16364	0.00167	2512	28	2540	65	2494	17	-2.2
	A15	0	61304	10.3870	0.31	0.45792	0.016	0.946	0.16475	0.00191	2470	27	2432	70	2505	20	3.6
	A16	0	122070	10.7212	0.32	0.47442	0.016	0.945	0.16353	0.00178	2499	27	2505	68	2492	18	-0.5
	A17	0	235243	10.3771	0.31	0.46042	0.015	0.948	0.16357	0.00169	2469	27	2443	66	2493	17	2.5
	A19	0	230013	10.4917	0.31	0.46654	0.016	0.954	0.16318	0.00166	2479	27	2470	68	2489	17	1.0
	A25	0	181355	10.4539	0.31	0.45542	0.015	0.951	0.16611	0.00176	2475	27	2421	68	2519	18	4.7
	Gr 5	0	311353	10.3468	0.31	0.46246	0.015	0.951	0.16210	0.00166	2466	27	2452	66	2478	17	1.3
	Gr 6	0	411631	10.6636	0.32	0.47220	0.018	0.975	0.16475	0.00179	2494	27	2495	78	2505	18	0.6
	Gr 11	0	102462	10.4451	0.31	0.46330	0.018	0.981	0.16383	0.00174	2475	27	2456	78	2496	18	2.0
	Gr 15	0	111636	10.5347	0.32	0.46282	0.018	0.985	0.16530	0.00186	2483	27	2454	80	2511	19	2.8
	Gr 20	0	284154	11.9029	0.36	0.49568	0.016	0.950	0.17519	0.00182	2596	28	2597	70	2608	17	0.6
	Gr 22	0	540185	11.9916	0.36	0.50031	0.020	0.994	0.17420	0.00180	2603	28	2617	85	2598	17	-0.8
	Gr 23	0	436162	10.6498	0.32	0.46502	0.015	0.943	0.16677	0.00174	2493	27	2464	64	2525	18	3.0
	Gr 27	0	220564	10.6494	0.32	0.47124	0.021	0.687	0.16422	0.00175	2493	27	2491	90	2500	18	0.5

The quoted errors are reported at 2-sigma, and represent the propagation of the measurment error and the external reproducibility (±3% relative for $^{207}Pb/^{235}U$ and $^{206}Pb/^{238}U$ and ±1% relative for $^{207}Pb/^{206}Pb$). ^{204}Pb (cps) when reported at 0 have been manually set. This protocol is based on the degree of correlation between the measured ^{207}Pb/206Pb and the ^{204}Pb (cps). When the degree of correlation is good (ie. R2 > 90%) the ^{204}Pb is considered real and is included in the calculation. As zircon commonly contains little to no common lead this is not often the case. When the $^{207}Pb/^{206}Pb$ vs. ^{204}Pb (cps) correlation is poor the ^{204}Pb is considered machine artifact or introduced and the levels are zeroed.

* Data from Schultz et al. in press

† Analyses not used in age treatments

Appendix 2
Wholerock geochemistry for rocks collected from the Queen Maud Block and Rae Domain

Sample ID:	ST-1B	ST-2	ST-2A	ST-4	ST-5	ST-6	ST-7	NT-3A	NT-3B
Domain	QMB	QMB	QMB	QMB	QMB	QMB	QMB	QMB	QMB
wt. %									
SiO_2	67.97	72.16	63.63	61.33	66.88	64.74	59.67	65.46	59.11
TiO_2	1.19	0.35	0.86	0.84	0.39	0.99	0.66	0.63	0.46
Al_2O_3	13.41	14.09	16.26	17.00	16.45	14.55	16.56	15.82	17.61
FeO_T	5.53	2.34	5.18	6.98	3.49	7.91	5.90	5.21	7.93
MnO	0.08	0.03	0.07	0.10	0.05	0.11	0.13	0.07	0.13
MgO	1.45	0.71	1.52	3.09	1.46	2.42	3.25	1.40	2.01
CaO	4.69	2.31	4.30	5.47	4.57	4.08	6.09	3.69	4.96
Na_2O	2.95	2.86	3.54	2.80	4.08	4.25	3.87	3.85	5.04
K_2O	1.70	4.78	3.80	1.86	1.77	0.72	2.81	3.51	1.50
P_2O_5	0.29	0.10	0.28	0.19	0.15	0.12	0.39	0.17	0.30
LOI	0.81	0.26	0.34	0.30	0.39	0.07	0.63	0.22	0.21
TOTAL	100.06	100.00	99.77	99.95	99.67	99.98	99.94	100.02	99.26
ppm									
Cr	0	0	0	62	45	24	31	0	0
Ni	0	0	0	40	29	23	12	0	0
Co	45	46	40	48	57	59	41	46	43
Sc	13	8	17	24	9	17	18	16	8
V	52	27	65	105	50	173	111	61	61
Cu	0	0	0	23	21	22	15	0	0
Pb	27	24	19	11	24	12	14	8	22
Zn	118	58	78	74	63	116	81	61	111
Rb	34	135	63	74	32	9	52	83	22
Cs	0.3	0.2	0.1	1.9	0.1	0.0	0.0	1.4	0.2
Ba	623	838	1960	743	723	415	1470	1120	583
Sr	473	269	464	322	552	367	951	327	397
Tl	0.21	0.77	0.38	0.42	0.22	0.08	0.33	0.33	0.16
Ga	18	17	20	21	20	22	20	22	26
Ge	1.0	1.1	1.0	1.1	1.0	1.2	1.1	1.1	1.5
Ta	1.46	1.89	1.21	1.42	1.79	2.40	0.93	1.28	0.64
Nb	13.4	5.2	11.4	10.2	7.2	10.2	10.4	10.8	2.8
Hf	12.9	4.5	8.3	5.1	4.8	3.8	5.1	7.5	7.3
Zr	453	144	306	163	159	119	172	257	265
Y	11.5	11.4	22.2	13.5	7.2	15.3	24.1	28.9	18.7
Th	1.4	1.7	0.2	2.3	2.5	4.0	0.4	5.2	2.0
U	0.63	0.33	0.30	0.98	4.12	4.31	0.22	1.95	0.88
La	30.7	50.4	40.7	27.0	27.3	17.5	41.6	48.7	69.4
Ce	62.8	94.7	87.8	55.1	51.5	34.6	100.1	100.5	131.1
Pr	7.24	10.30	11.26	6.39	5.53	3.74	13.19	11.67	13.76
Nd	28.42	36.62	48.45	24.46	19.83	14.21	52.87	45.07	50.05
Sm	4.76	5.71	9.27	4.56	3.08	3.00	9.53	9.12	8.21
Eu	1.96	1.29	2.93	1.49	1.25	0.97	2.01	2.05	2.16
Gd	4.00	4.20	7.73	3.97	2.28	3.18	7.27	7.60	6.12
Tb	0.50	0.53	1.02	0.55	0.27	0.54	0.94	1.16	0.84
Dy	2.53	2.74	5.07	2.87	1.41	3.07	4.80	5.78	3.89
Ho	0.46	0.46	0.88	0.55	0.27	0.60	0.91	1.11	0.72
Er	1.25	1.25	2.30	1.59	0.77	1.84	2.78	3.28	2.02
Tm	0.175	0.163	0.303	0.235	0.115	0.275	0.419	0.470	0.285
Yb	1.17	0.99	1.80	1.54	0.81	1.67	2.52	2.91	1.81
Lu	0.183	0.141	0.259	0.234	0.142	0.253	0.363	0.423	0.278

Sample ID:	NT-3C	NT-4b	NT-7	NT-7A	ST-1A	NT-0A	NT-1	NT-5	BT-0
Domain	QMB	QMB	QMB	QMB	Rae	Rae	Rae	Rae	Rae
wt. %									
SiO_2	65.43	68.37	65.39	66.45	73.19	77.19	60.39	74.42	70.03
TiO_2	0.61	0.54	1.01	1.14	0.17	0.15	0.60	0.11	0.31
Al_2O_3	15.28	15.05	14.31	14.52	14.22	12.43	19.58	13.63	14.76
FeO_T	5.37	3.91	7.52	8.32	1.63	1.40	4.28	0.93	2.78
MnO	0.17	0.05	0.11	0.11	0.02	0.02	0.06	0.01	0.04
MgO	1.48	1.01	0.98	1.24	0.49	0.49	1.53	0.25	1.15
CaO	3.82	3.26	3.46	3.39	2.22	2.21	6.15	1.27	1.94
Na_2O	4.37	3.57	2.24	2.12	4.08	3.42	4.65	2.78	2.44
K_2O	2.55	3.78	4.55	2.34	3.05	2.16	1.58	6.07	5.86
P_2O_5	0.20	0.15	0.32	0.35	0.05	0.08	0.19	0.07	0.10
LOI	0.17	0.22	0.10	0.03	0.61	0.42	1.04	0.36	0.52
TOTAL	99.45	99.90	99.97	100.00	99.75	99.97	100.05	99.89	99.91
ppm									
Cr	0	0	0	0	0	0	0	0	0
Ni	21	0	0	0	0	0	0	0	0
Co	48	51	53	66	63	57	39	59	60
Sc	24	12	23	25	4	4	10	3	7
V	48	43	35	41	15	18	57	10	37
Cu	0	14	47	21	10	0	0	0	0
Pb	12	15	17	12	21	21	18	42	23
Zn	73	41	121	163	33	0	68	0	35
Rb	39	77	116	73	45	63	54	116	145
Cs	0.3	0.5	0.6	0.4	0.3	2.6	1.1	0.0	1.4
Ba	705	1740	1530	1270	1070	533	973	1470	860
Sr	239	339	195	200	632	352	871	315	293
Tl	0.20	0.37	0.75	0.47	0.24	0.36	0.37	0.69	0.80
Ga	20	19	22	24	16	15	23	16	18
Ge	1.4	1.0	1.5	1.6	0.8	0.8	1.0	1.0	1.0
Ta	1.34	1.29	2.55	3.24	1.57	1.87	1.16	1.22	1.71
Nb	12.2	8.3	25.5	32.0	2.8	11.2	7.1	2.1	6.3
Hf	9.3	6.2	9.1	12.5	2.8	2.5	6.0	1.8	3.7
Zr	320	210	317	440	89	77	223	58	120
Y	18.0	26.7	41.5	26.1	2.4	8.5	15.9	2.1	9.2
Th	2.2	4.1	4.4	2.4	10.2	13.6	5.0	8.4	13.6
U	1.26	0.70	0.71	1.58	0.63	5.20	1.93	0.28	1.67
La	39.7	57.7	50.8	42.3	42.5	39.0	43.8	33.5	45.0
Ce	81.0	122.8	113.2	97.3	80.8	77.4	92.1	64.0	88.5
Pr	9.26	14.23	13.76	12.06	8.41	8.67	11.01	6.16	8.88
Nd	35.59	54.68	55.35	49.10	27.79	29.89	43.95	19.75	28.73
Sm	6.78	10.94	11.43	10.40	3.13	4.96	7.85	2.85	4.72
Eu	1.61	1.95	2.57	2.67	1.11	1.01	2.39	0.93	0.96
Gd	5.67	8.86	10.21	8.67	1.56	3.45	5.98	1.48	2.96
Tb	0.80	1.28	1.59	1.20	0.14	0.42	0.72	0.14	0.40
Dy	3.84	6.13	8.18	5.74	0.60	1.98	3.51	0.49	1.92
Ho	0.70	1.10	1.61	1.05	0.09	0.31	0.61	0.07	0.34
Er	2.02	3.03	4.98	3.00	0.24	0.82	1.65	0.20	0.92
Tm	0.298	0.395	0.743	0.394	0.036	0.112	0.231	0.029	0.127
Yb	1.88	2.36	4.65	2.62	0.25	0.70	1.44	0.20	0.80
Lu	0.302	0.325	0.741	0.441	0.038	0.096	0.207	0.035	0.115

Sample ID:	BT-1	BT-1A	BT-2	BT-3	BT-4	JT-2	JT-3	JT-4	JT-5A
Domain	Rae	Rae	Rae	Rae	Rae	Rae	Rae	Rae	Rae
wt. %									
SiO_2	73.40	69.80	68.18	60.33	64.50	62.01	72.16	67.74	70.65
TiO_2	0.17	0.31	0.42	0.55	0.73	0.64	0.24	0.41	0.29
Al_2O_3	14.86	15.22	15.62	18.19	15.33	17.58	13.72	15.58	15.25
FeO_T	1.52	3.02	3.87	5.18	5.80	5.25	1.88	3.47	2.46
MnO	0.02	0.04	0.06	0.07	0.07	0.07	0.04	0.06	0.02
MgO	0.68	1.28	1.51	2.35	1.77	1.99	0.82	1.30	0.99
CaO	1.25	2.38	3.10	5.75	3.18	4.47	0.82	3.17	2.46
Na_2O	3.55	2.93	3.43	4.06	3.42	3.64	3.10	3.66	3.83
K_2O	3.64	3.92	3.00	2.42	3.36	2.83	5.71	3.80	3.29
P_2O_5	0.10	0.09	0.12	0.21	0.34	0.19	0.08	0.18	0.08
LOI	0.78	0.81	0.61	0.77	0.81	0.69	0.82	0.40	0.50
TOTAL	99.97	99.79	99.92	99.88	99.30	99.36	99.38	99.78	99.82
ppm									
Cr	0	0	0	23	0	0	0	0	0
Ni	0	0	0	0	0	25	0	0	0
Co	54	70	42	44	37	40	48	46	58
Sc	4	8	10	13	10	12	5	8	4
V	18	43	58	82	74	81	18	44	28
Cu	0	0	0	10	19	0	0	0	0
Pb	24	28	25	10	11	17	19	22	28
Zn	32	59	74	50	80	81	32	51	51
Rb	131	133	102	60	121	122	148	111	117
Cs	6.5	5.1	5.7	1.6	2.1	7.4	1.4	1.3	2.0
Ba	638	905	626	1210	1180	893	1140	1680	710
Sr	247	327	441	802	427	450	189	559	338
Tl	0.94	0.90	0.80	0.27	0.76	0.89	0.94	0.72	0.83
Ga	20	21	22	23	21	25	15	17	20
Ge	1.0	1.2	1.3	1.0	1.1	1.2	1.3	1.1	1.0
Ta	1.63	1.83	1.41	1.03	1.12	1.28	2.02	1.32	1.63
Nb	5.0	5.7	7.5	7.1	8.5	10.2	10.0	6.9	5.9
Hf	1.8	3.1	3.6	4.9	7.6	5.8	4.1	4.2	2.4
Zr	53	96	116	181	291	211	132	150	76
Y	6.6	10.1	13.6	18.7	17.5	13.2	10.2	9.5	11.1
Th	9.0	11.7	12.9	4.7	12.4	12.1	23.7	13.6	16.0
U	1.98	3.76	3.61	1.09	1.37	5.13	5.30	2.72	1.56
La	25.3	32.9	36.3	40.3	99.7	53.2	66.1	67.1	32.7
Ce	50.1	67.6	76.6	90.1	206.1	109.2	130.0	130.3	70.9
Pr	5.14	7.23	8.30	10.96	21.84	12.16	13.08	13.13	7.95
Nd	17.89	25.71	29.71	43.19	74.18	43.62	42.09	42.86	28.98
Sm	3.23	4.81	5.70	8.74	10.98	7.50	6.07	6.21	5.82
Eu	0.84	1.05	1.11	2.26	1.98	1.67	1.27	1.61	0.89
Gd	2.27	3.40	3.92	6.38	6.95	4.93	3.50	3.53	4.09
Tb	0.29	0.47	0.57	0.84	0.79	0.58	0.43	0.42	0.50
Dy	1.28	2.11	2.81	3.76	3.48	2.64	1.96	1.87	2.23
Ho	0.23	0.36	0.51	0.68	0.61	0.47	0.33	0.33	0.38
Er	0.65	1.02	1.48	1.82	1.58	1.27	0.94	0.90	1.07
Tm	0.094	0.148	0.220	0.251	0.223	0.177	0.142	0.132	0.154
Yb	0.61	0.96	1.37	1.63	1.40	1.18	1.09	0.95	0.98
Lu	0.081	0.134	0.212	0.236	0.202	0.173	0.173	0.146	0.151

Sample ID:	MS-1143	MS-1152	ST-1	ST-2B	ST-6A	NT-3	NT-8A
Domain	Rae	Rae	QMB	QMB	QMB	QMB	QMB
wt. %							
SiO_2	70.67	67.28	46.07	49.73	48.88	49.71	47.28
TiO_2	0.51	0.35	2.38	0.80	2.64	0.74	3.60
Al_2O_3	14.00	15.93	14.68	10.58	12.07	15.19	13.44
FeO_T	3.73	3.58	15.25	16.22	17.02	9.87	16.97
MnO	0.04	0.05	0.18	0.27	0.27	0.16	0.31
MgO	0.77	1.55	5.56	12.90	4.16	8.11	6.08
CaO	1.98	3.31	9.36	7.79	8.94	10.54	9.52
Na_2O	3.17	3.42	2.69	1.41	3.29	2.98	0.51
K_2O	4.35	3.22	0.89	0.20	0.49	0.97	1.37
P_2O_5	0.20	0.15	1.48	0.18	0.20	0.14	0.37
LOI	0.39	0.55	1.03	-0.05	-0.30	1.51	0.58
TOTAL	99.80	99.41	99.58	100.01	97.65	99.92	100.02
ppm							
Cr	0	50	43	385	0	424	80
Ni	0	0	50	148	0	83	50
Co	46	51	74	65	40	56	70
Sc	8	13	34	46	36	35	46
V	29	40	411	186	371	229	578
Cu	0	0	51	16	15	33	29
Pb	32	38	8	0	0	0	0
Zn	58	49	127	134	52	86	157
Rb	220	97	20	3	3	16	20
Cs	4.3	0.5	0.4	0.0	0.1	0.3	0.3
Ba	420	854	450	159	186	275	87
Sr	157	331	549	325	160	295	276
Tl	1.67	0.92	0.15	0.00	0.00	0.09	0.12
Ga	20	19	22	13	20	16	26
Ge	1.1	1.2	1.3	1.5	1.1	1.2	2.0
Ta	2.22	1.50	1.36	0.46	1.76	0.45	1.69
Nb	16.3	7.9	13.5	2.9	16.0	3.8	19.0
Hf	6.1	4.1	4.0	1.3	4.2	1.6	5.0
Zr	196	122	143	37	126	51	166
Y	13.8	13.4	30.1	15.4	35.7	15.5	42.0
Th	27.0	21.3	0.7	0.2	0.8	1.5	0.6
U	3.33	1.93	0.43	0.04	0.39	0.41	0.41
La	77.1	47.2	55.6	11.1	16.8	16.3	16.2
Ce	160.5	96.6	130.3	29.2	42.2	37.3	45.0
Pr	16.62	10.16	16.11	4.20	5.76	4.57	6.37
Nd	55.34	35.54	68.25	19.23	25.60	18.65	30.16
Sm	9.04	6.74	12.23	4.38	6.70	3.92	8.57
Eu	1.06	1.25	3.62	1.13	2.30	1.24	2.49
Gd	5.64	4.81	10.56	4.15	7.98	3.54	9.23
Tb	0.68	0.63	1.35	0.60	1.34	0.57	1.56
Dy	3.02	2.87	6.82	3.36	7.57	3.06	8.70
Ho	0.49	0.52	1.20	0.65	1.43	0.60	1.68
Er	1.34	1.41	3.24	1.91	4.42	1.84	4.98
Tm	0.178	0.180	0.436	0.284	0.632	0.268	0.718
Yb	1.07	1.13	2.69	1.82	3.72	1.72	4.32
Lu	0.146	0.153	0.405	0.281	0.546	0.268	0.640

Appendix 3
UTM locations for rocks collected from the Queen Maud Block and Rae Domain

Sample ID:	Zone	Eastings	Northings
BT0	15	384006	7450694
BT1	14	627018	7460276
BT2	14	612176	7477230
BT3	14	601052	7484480
BT4	14	593481	7494117
BT5	14	570632	7517875
NT0	14	603895	7466022
NT1	14	582951	7460491
NT2	14	576069	7464526
NT3	14	568109	7473881
NT4	14	560705	7477556
NT5	14	556670	7480316
NT6	14	552965	7484413
NT7	14	545037	7488941
NT8	14	536346	7499093
ST1	14	543363	7453994
ST2	14	539091	7460056
ST3	14	515891	7466480
ST4	14	489438	7470884
ST5	14	478881	7481896
ST6	14	471911	7487529
ST7	14	462688	7498035
JT1	15	441668	7453207
JT2	15	412615	7465615
JT3	15	396800	7476600
JT4	15	393000	7478200
JT5	15	389388	7483903
MS4-1143	15	488394	7452248
MS4-1152	15	462677	7464220

All locations were taken using the NAD 87 datum